Global and Planetary Change 166 (2018) 62–74

Contents lists available at ScienceDirect

Global and Planetary Change

journal homepage: www.elsevier.com/locate/gloplacha

Research article

Ocean as the main driver of Antarctic ice sheet retreat during the Holocene

Xavier Crosta[a,*], Julien Crespin[b,a], Didier Swingedouw[a], Olivier Marti[c], Valérie Masson-Delmotte[c], Johan Etourneau[d], Hugues Goosse[e], Pascale Braconnot[c], Ruth Yam[b], Irena Brailovski[b], Aldo Shemesh[b]

[a] EPOC, UMR CNRS 5805, Université de Bordeaux, 33405 Talence, France
[b] EPS, Weizmann Institute of Science, Rehovot 76100, Israel
[c] LSCE, UMR CEA-CNRS-UVSQ 8212, Université Paris Saclay, Gif-sur-Yvette, France
[d] Instituto Andaluz de Ciencias de la Tierra, CSIC-Universidad Granada, Granada, Spain
[e] Université Catholique de Louvain, Georges Lemaitre Centre for Earth and Climate Research, Louvain-la-Neuve, Belgium

A B S T R A C T

Ocean-driven basal melting has been shown to be the main ablation process responsible for the recession of many Antarctic ice shelves and marine-terminating glaciers over the last decades. However, much less is known about the drivers of ice shelf melt prior to the short instrumental era. Based on diatom oxygen isotope ($\delta^{18}O_{diatom}$; a proxy for glacial ice discharge in solid or liquid form) records from western Antarctic Peninsula (West Antarctica) and Adélie Land (East Antarctica), higher ocean temperatures were suggested to have been the main driver of enhanced ice melt during the Early-to-Mid Holocene while atmosphere temperatures were proposed to have been the main driver during the Late Holocene. Here, we present a new Holocene $\delta^{18}O_{diatom}$ record from Prydz Bay, East Antarctica, also suggesting an increase in glacial ice discharge since ~4500 years before present (~4.5 kyr BP) as previously observed in Antarctic Peninsula and Adélie Land. Similar results from three different regions around Antarctica thus suggest common driving mechanisms. Combining marine and ice core records along with new transient accelerated simulations from the IPSL-CM5A-LR climate model, we rule out changes in air temperatures during the last ~4.5 kyr as the main driver of enhanced glacial ice discharge. Conversely, our simulations evidence the potential for significant warmer subsurface waters in the Southern Ocean during the last 6 kyr in response to enhanced summer insolation south of 60°S and enhanced upwelling of Circumpolar Deep Water towards the Antarctic shelf. We conclude that ice front and basal melting may have played a dominant role in glacial discharge during the Late Holocene.

1. Introduction

Understanding the mechanisms of recent regional climate variability is particularly challenging for Antarctica and the Southern Ocean (SO) due to complex interactions of the different components of the Earth's climate system, short instrumental records and heterogeneous climatic trends observed over the last decades (Jones et al., 2016; Turner et al., 2016). Indeed, no significant trends in surface air temperature (SAT) have been observed above East Antarctica (EA) in contrast to the remarkably fast atmospheric warming (~3 °C since 1951; Turner et al., 2005; Chapman and Walsh, 2007) and oceanic warming (>1 °C since 1955; Meredith and King, 2005) reported in the Antarctic Peninsula (AP) region where retreat of marine glacier fronts has been evidenced over the past six decades (Cook et al., 2005; Rignot et al., 2013). Conversely, the complex structure of recent EA glacier variations may arise from dynamical calving rather than basal melting and there is so far no robust evidence of an EA fingerprint of human-induced climate change (Pritchard et al., 2009; Miles et al., 2013). The respective roles of atmosphere and ocean on recent glacier and ice-shelf dynamics around Antarctica remain poorly understood, preventing robust attribution. Recent modelling studies related Antarctic ice loss either to atmospheric or oceanic forcing. Atmospheric warming may increase hydrofracturing of buttressing ice-shelves and structural collapse of marine-terminating ice cliffs (DeConto and Pollard, 2016) piling up onto oceanic warming and increasing intrusion of warm waters on the Antarctic continental shelf (Smith et al., 2017; Walker and Gardner, 2017) as the prime mechanism to produce a large and rapid dynamical ice-sheet response (Golledge et al., 2015; Ritz et al., 2015; Obase et al., 2017). In response to increased future greenhouse gases emission (RCP8.5 scenarios, corresponding to > 3 °C global warming

* Corresponding author.
E-mail address: xavier.crosta@u-bordeaux.fr (X. Crosta).

https://doi.org/10.1016/j.gloplacha.2018.04.007
Received 8 January 2018; Received in revised form 16 April 2018; Accepted 30 April 2018
Available online 09 May 2018
0921-8181/

above late 20th century levels), new ice sheet-ice shelf models representing crudely such processes simulate large melting of several Antarctic sectors, corresponding to estimated contributions of the Antarctic ice sheet to global mean sea-level rise ranging from ~40 cm (Golledge et al., 2015) to > 1 m (DeConto and Pollard, 2016) by the end of the 21st century, and several meters in the following centuries. The projected freshening of the SO is expected to affect the global ocean circulation (Swingedouw et al., 2008, 2009; Williams et al., 2016; Bakker et al., 2017), with potentially major implications for heat and carbon uptakes as well as for projected climate patterns at the global scale (Barnes et al., 2009).

Given the potential major implications of Antarctic ice discharge, and the remaining uncertainties on the ability of models to correctly represent key processes, it is important to learn from past changes. As instrumental and historical records are very short and scarce around Antarctica (Jones et al., 2016), paleoclimate records provide a unique opportunity to describe the baseline conditions before the industrial-era warming (Abram et al., 2016) and to expand the current understanding of mechanisms underlying temporal and regional differences in circum-Antarctic climate change on centennial and longer timescales. Proxy records from natural archives document throughout the Holocene spatially heterogeneous trends in air temperature over Antarctica (Masson et al., 2000; Mayewski et al., 2009; Masson-Delmotte et al., 2011), sea-surface temperature (SST) and sea ice (Cunningham et al., 1999; Allen et al., 2010; Denis et al., 2010; Kim et al., 2012; Etourneau et al., 2013; Peck et al., 2015) as well as ice sheet and glacier fluctuations on multi-decadal to millennial timescales (Ingólfsson et al., 1998; Hodgson et al., 2009; Verleyen et al., 2011; Bentley and The Raised Consortium, 2014). However, the causes for these spatial variations are not yet fully understood. In this context, documenting the history of glacial ice discharge (iceberg and brash-ice discharge together with liquid water from basal and frontal melting of floating glaciers-ice shelves) to coastal Antarctic waters and the potential drivers of this discharge (oceanic and atmospheric changes, including seasonal aspects) is crucial to estimate the sensitivity of marine-based glaciers and ice shelves to atmospheric and oceanic temperatures.

Here we generated a new high-resolution record of $\delta^{18}O_{diatom}$ from Prydz Bay (PB) in East Antarctica and combined it to previously published ones from the western Antarctic Peninsula (WAP) (Pike et al., 2013) and Adélie Land (AL) (Crespin et al., 2014) in order to characterize the magnitude and geographical extent of glacial ice discharge changes around Antarctica over the last 9 kyr. Using marine and ice core records of temperatures and sea-ice conditions along with new transient simulations from the IPSL-CM5A-RL climate model, we place the diatom oxygen isotope records in regional climatic and oceanographic context to assess the main drivers of circum-Antarctic ice discharge during the Holocene.

2. Oceanographic settings

Prydz Bay (PB) is located in the Indian sector of the SO, East Antarctic Margin, between approximately 70° E and 80° E (Fig. 1). PB encompasses the largest drainage system of the East Antarctic ice sheet (O'Brien et al., 2007) through the Lambert glacier and Amery Ice Shelf (Harris et al., 1998), which release vast amounts of freshwater and terrigenous particles in PB.

The ocean circulation in PB is mainly governed by a large cyclonic gyre entering PB to the East, subsequently merging with the westward flowing Antarctic Coastal Current that runs along the Amery Ice Shelf and exiting PB to the West (Smith and Tréguer, 1994; Nunes-Vaz and Lennon, 1996; Herraiz-Borreguero et al., 2015). Relatively warm and salty Circumpolar Deep Water (CDW), initially transported as part of the Antarctic Circumpolar Current, upwells onto the continental shelf via several troughs incising the continental shelf (Walker et al., 2007; Walker and Gardner, 2017). The inflow of CDW peaks in winter and flows southward at 200–400 m deep within the gyre (Liu et al., 2017). The CDW is modified (mCDW) along its journey to the subice cavity below the Amery Ice Shelf where the annual mean heat transport of $\sim 25 \times 10^{11}$ J·s^{-1} promotes basal melting (Liu et al., 2017). The inflow of mCDW was shown to drive a net basal melt rate of up to 260.5 m yr^{-1} in 2001 (Herraiz-Borreguero et al., 2015).

Sea ice extends to approximately 58°S during winter and generally retreats back to the continent during summer, though the intermittent presence of iceberg fields in the eastern PB via the inflow of Antarctic Coastal Current (Smith et al., 1984; Worby et al., 1998) favours sea-ice formation. Sea-ice duration in eastern PB is ~10–11 months per year compared to ~9–10 months per year in western PB (Smith et al., 1984).

3. Material and methods

3.1. Sediment material and chronology

Piston core NBP0101-JPC24 (68°41.64′S, 76°42.71′E; 816 m water depth; hereafter referred to JPC24) was retrieved from the slope of one of the depressions composing eastern PB during the NBP0101 – CHAOS cruise (Fig. 1) (Leventer et al., 2006). Core JPC24 is a 17 m-long sequence of diatom oozes. The age model is based on six radiocarbon dates corrected for the local marine reservoir age of 1280 yr ± 200 yr (Leventer et al., 2006). The core covers the last 11 kyr BP with mean accumulation rate of ~0.30 cm/yr from 11 kyr to 7.5 kyr and a mean sedimentation rate of ~0.10 cm/yr afterward. A detailed description of core JPC24 stratigraphic framework and age model is presented in Leventer et al. (2006) and Barbara et al. (2010).

3.2. Oxygen isotopes in diatoms

Previous studies have shown that $\delta^{18}O_{diatom}$ in SO sedimentary records reflect changes in the $\delta^{18}O$ of the seawater in which the diatoms grow (Shemesh et al., 1992; Swann and Leng, 2009; Swann et al., 2013; Pike et al., 2013) coupled with a minor temperature effect. In Antarctic coastal environments, the injection of highly ^{18}O-depleted glacial solid ice (upon melting of solid ice in coastal Antarctic) and liquid melt is the sole process that can significantly alter the $\delta^{18}O_{seawater}$ (Meredith et al., 2010, 2013. Solid ice discharge and frontal melt will directly influence the $\delta^{18}O_{seawater}$ of surface waters (Meredith et al., 2010) while basal meltwater formed at depth needs first to be transported upward. Observations show that buoyant Ice Shelf Water generally reaches the ocean surface as soon as they emerge from the ice shelf cavity (Mahoney et al., 2011). By contrast, a recent modelling study suggests that, for modern conditions in the Bellinghausen Sea, the core of the Ice Shelf Water lies at ~100 m deep, below the horizon in which diatoms thrive (Regan et al., 2018). According to this study, only a part of basal meltwater diffuses upward to reach the surface, which is still sufficient to significantly influence the surface $\delta^{18}O_{seawater}$. Unfortunately, the $\delta^{18}O_{diatom}$ proxy cannot make the difference between these two ablation processes. Although some solid ice can be calved from growing glaciers, we believe that only receding glaciers and ice shelves can inject enough solid ice and meltwater to significantly lower the surface $\delta^{18}O_{seawater}$ and, therefore, the $\delta^{18}O_{diatom}$ values. This interpretation is supported by several studies. Analyzing mono-generic diatom assemblages preserved in deglacial laminae in core ODP 1098 off western Antarctic Peninsula, Swann et al. (2013) demonstrated that summer diatoms bear a lower $\delta^{18}O_{diatom}$ signal than spring diatoms in relation to peak glacial discharge and melt during the summer season. Based on this finding, Pike et al. (2013) interpreted the lowest $\delta^{18}O_{diatom}$ values recorded in core OPD 1098 as events of strong glacial recession during the Holocene that were previously assessed via sedimentological analyses.

Diatom oxygen isotopes in core JPC24 have been purified and analyzed from sediment spanning the last 9 kyr to document Holocene changes in glacial discharge after the main deglaciation of PB (Mackinstosh et al., 2011). Samples from core JPC24 were analyzed

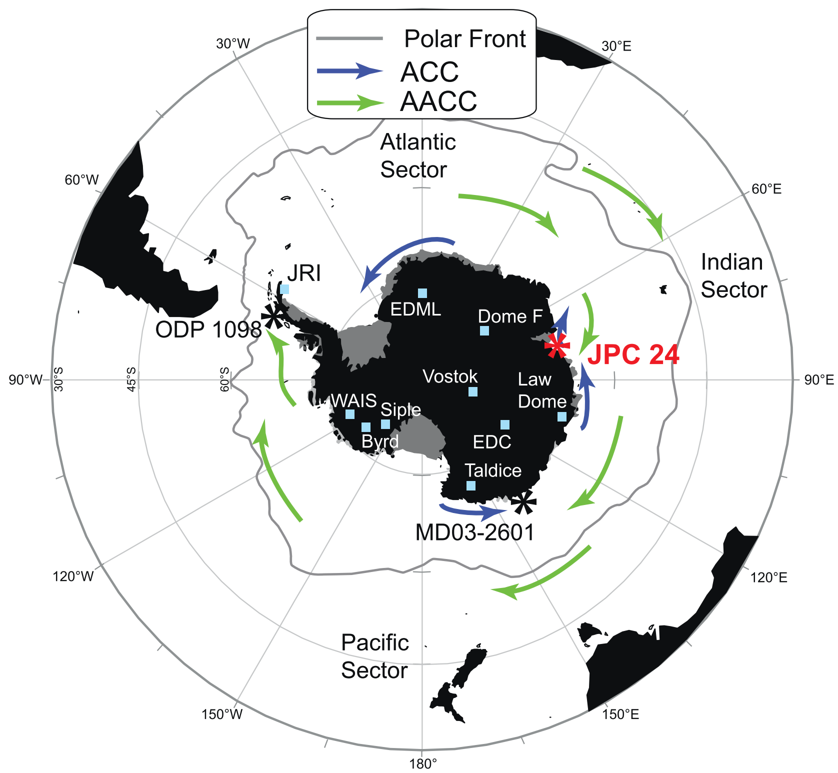

Fig. 1. Locations of oceanic cores JPC24 (this study, red asterisk), ODP 1098 (Pike et al., 2013) and MD03-2601 (Crespin et al., 2014) (black asterisks) where $\delta^{18}O_{diatom}$ records are available, and locations of ice core drilling sites where Holocene records are available and discussed in this manuscript (light blue squares), along with large scale oceanographic circulation in the Southern Ocean. ACC: Antarctic Coastal Current; AACC: Antarctic Circumpolar Current, from Orsi et al., 1995). (For interpretation of the references to colour in this figure legend, the reader is referred to the web version of this article.)

every 20 cm providing a ~200 years resolution. Samples were cleaned and analyzed for $\delta^{18}O_{diatom}$ analysis following Crespin et al. (2014).

Previous in-situ studies have demonstrated that it is necessary to work on a restricted diatom size fraction to avoid potential size fraction effects (Swann et al., 2008) and contamination by other siliceous organisms, such as radiolarians and sponges that might have different fractionation factors. We however note that two $\delta^{18}O_{diatom}$ and $\delta^{18}O_{radiolarian}$ deep-sea records from the Atlantic sector of the SO present very similar patterns and absolute values over the last 30 kyrs (Abelmann et al., 2015). Large *Coscinodiscus* and *Actinocyclus* are known to adjust their buoyancy and may therefore precipitate their frustule in deeper water masses having a different $\delta^{18}O_{seawater}$ signal. They may also present a different fractionation factor (Swann et al., 2008). To avoid contamination by large diatoms and non-diatom siliceous organisms we here selected diatoms in the 10–32 μm size fraction. The main diatom species preserved in the 10–32 μm size fraction are *Fragilariopsis curta* and *F. rhombica* thriving in spring, *F. kerguelensis* and small *Thalassiosira lentiginosa* thriving in summer and *Thalassiosira antarctica* thriving in summer-autumn. These species are the dominant diatoms in core JPC24 and MD03–2601 (Denis et al., 2010; Crosta et al., 2007, 2008) implying a very small alteration of the original diatom assemblages and ensuring a mixed assemblage of surface-living diatoms in the cleaned samples. It is however probable that the dominance of each diatom species in the cleaned samples varied according to their dominance in the raw samples. Diatom census counts indicate that summer-autumn diatoms dominated the mid-Holocene warm period during which *T. antarctica*, *F. kerguelensis* and *T. lentiginosa* altogether amounted 40–50% of the total diatom assemblages while spring developing *F. curta* and *F. rhombica* represented 15–25%. Conversely, the spring diatoms accounted for 30–50% of the total diatom assemblages while the summer-autumn diatoms dropped to ~15% during the colder Neoglacial period (Denis et al., 2010; Crosta et al., 2007, 2008). The relative abundances of large *Coscinodiscus* and *Actinocyclus* in cores JPC24 and MD03–2601 are < 5% throughout cores (unpublished data).

It is important to note that the selected diatoms in the cleaned samples may bear a seasonal shift from summer-autumn to spring between the mid- and late Holocene periods, respectively, that cannot explain the light $\delta^{18}O_{diatom}$ values during the late Holocene recorded in cores JPC24 and MD03-2601. Indeed, Swann et al. (2013) demonstrated that summer diatoms present a light $\delta^{18}O$ signal compared to spring diatoms as increased glacial discharge occurs during the summer relative to the spring. If the $\delta^{18}O_{diatom}$ records were driven by changes in the diatom assemblages we should then expect heavier values during the Neoglacial compared to the Hypsithermal, in opposion to what is observed in the three records (Fig. 3A–C).

After the cleaning step, all samples were subjected to light microscopy (×1000 magnification) inspection in order to evaluate their purity prior to isotope analysis. Additionally, several cleaned samples along the core were examined using SEM in order to evaluate a possible dissolution effect and to ensure the purity of the samples. Such control showed that JPC24 diatoms are well preserved and do not exhibit signs of dissolution or diagenesis. It also showed that contamination by fragments of large diatoms and non-diatom siliceous organisms was very low.

More details on species effect, dissolution, silica maturation, sea-surface temperature and water mass changes of cores ODP 1098 and MD03-2601 can be found in Pike et al. (2013), Swann et al. (2013) and Crespin et al. (2014), respectively. The $\delta^{18}O_{diatom}$ measurements were performed using a Controlled Isotopic Exchange with two water samples having different isotopic compositions followed by Infra-Red (IR) laser fluorination extraction connected in line with isotope ratio mass spectrometer at the Weizmann Institute of Science, Israel. More information on the whole protocol can be found in Crespin et al. (2014). The isotope measurements were made on the 10–32 μm size fraction where most of the diatom assemblages lie. The $\delta^{18}O_{diatom}$ values are expressed relative to VSMOW and showed an analytical precision of ± 0.36‰ (1σ).

3.3. Ice cores: EOF analysis

We have performed an empirical orthogonal function (EOF) analysis

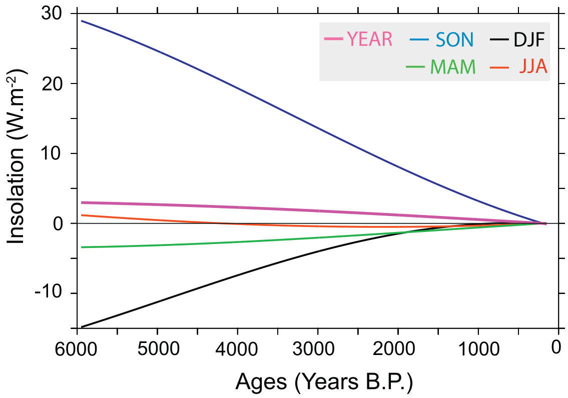

Fig. 2. Seasonal insolation change integrated over the 60–90°S region. In our accelerated 3-member ensemble simulations we only consider insolation change derived from Berger (1988) for the period 6 kyrs BP until present. The insolation changes averaged between 60 and 90°S is represented here as an anomaly compared to present-day conditions, with in pink the annual mean value, in red the Austral winter (average of June–July–August, JJA), in black the Austral summer (average of December–January–February, DJF), in blue the Austral spring (average of September–October–November, SON), in green the Austral autumn (average of March–April–May MAM). (For interpretation of the references to colour in this figure legend, the reader is referred to the web version of this article.)

Table 1
Description of the IPSL-CM5A-LR simulations considered.

	# Ensemble	Initial conditions	Forcing	Years of simulation
Control	1	Spin-up simulation	Pre-industrial	1 × 1000
Accelerated Holocene	3	Start every 10 years	Insolation[a]	3 × 600

[a] Berger (1988).

on a set of ten $\delta^{18}O$ ice core records (Dome F, West Antarctic Ice Sheet Divide, Byrd, Siple Dome, James Ross Island, EPICA Dome C, EPICA Dronning Maud Land, Vostok, Law Dome, TALDICE; Fig. 1) resampled every 200 years for the last 9 kyr. The EOF calculations were carried out with the AnalySeries software (Paillard et al., 1996). Data sets were extracted from the Pangaea (http://www.pangaea.de) and National Oceanic and Atmospheric Administration (NOAA) (ftp://ftp.ncdc.noaa.gov) websites.

3.4. IPSL-CM5A-LR simulations

The ocean-atmosphere coupled model used in this study is the IPSL-CM5A (Dufresne et al., 2013) in its low resolution (LR) version. The IPSL-CM5A-LR is based on the following model components: the LMDz atmospheric model (1.875° × 3.75°), the ORCHIDEE model of continental surfaces including carbon cycle, the ORCA2 ocean model (2° × (0.5–2°)) and the LIM2 sea-ice model. The simulations only account for astronomical forcing (Berger, 1988; Fig. 2), with no change in greenhouse gases, solar, and volcanic forcing.

Due to constrain on computing time, we considered here accelerated forcing i.e. the insolation is accelerated by a factor of 10, leading to 600-year simulations that represent the last 6 kyr. We did not consider any changes in greenhouse gas concentrations, fixed here at their pre-industrial values of 280 ppm for CO_2 (Dufresne et al., 2013) since they are relatively small over the Holocene. To remove part of the internal variability, we consider an ensemble of three- simulations, only differing by their initial conditions (Table 1).

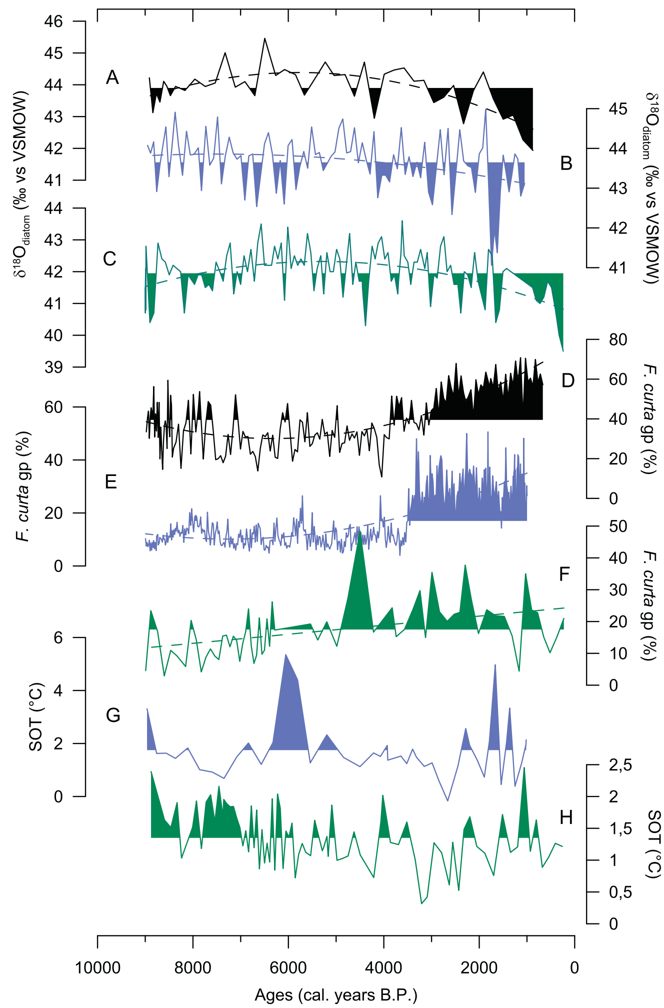

Fig. 3. Marine paleo-environnemental data. A: $\delta^{18}O_{diatom}$ record in core JPC24 from PB (black line; this study); B: $\delta^{18}O_{diatom}$ record in core MD03-2601 from AL (blue line; Crespin et al., 2014); C: $\delta^{18}O_{diatom}$ record in core ODP 1098 from the WAP (green line; Pike et al., 2013); D: relative abundance of the *Fragilariopsis curta* group in core JPC24 (black line; Denis et al., 2010); E: relative abundance of the *F. curta* gp in core MD03-2601 (blue line; Denis et al., 2010); F: relative abundance of the *F. curta* gp in core JPC10 from the WAP (green line; Etourneau et al., 2013); G: record of sub-surface ocean temperatures in core MD03-2601 (blue line; Kim et al., 2012); H: record of sub-surface ocean temperatures in core JPC10 (green line; Etourneau et al., 2013). In each plot, the shading represents the values that are below ($\delta^{18}O_{diatom}$) or above (*F. curta* and SOT) the mean value of the record. Dashed lines represent 2nd order polynome best fits to the records. (For interpretation of the references to colour in this figure legend, the reader is referred to the web version of this article.)

3.5. Model-data comparison

To compare the model results with the proxy data ($\delta^{18}O_{diatom}$, SST, ice core $\delta^{18}O$), we selected the closest point in the model grid to the considered core site, and used the mask of land or ocean, depending on the data.

4. Results and discussion

Previous studies have shown that the main control on $\delta^{18}O_{diatom}$ in the SO (Shemesh et al., 1992, 2002) and coastal Antarctic environments (Pike et al., 2013; Swann et al., 2013; Crespin et al., 2014) is a freshening of the sea-surface waters by $\delta^{18}O$-depleted solid ice and glacial meltwater, the signature of which is taken up by the diatoms. We thereafter interpret the $\delta^{18}O_{diatom}$ measured in the three marine cores

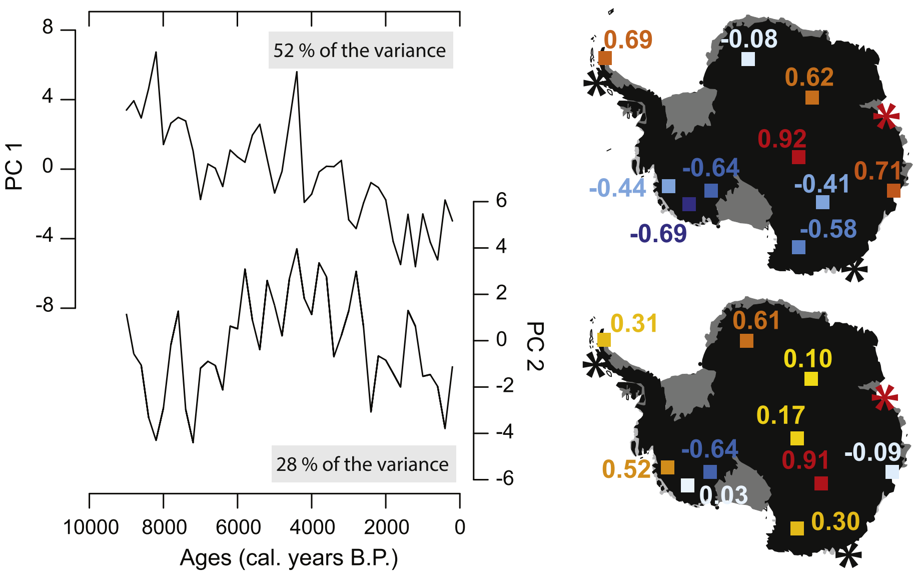

Fig. 4. First two PCs from ten $\delta^{18}O$ Antarctic ice core records (Dome F, Epica Dome C, West Antarctic Ice Sheet Divide, Byrd, Siple, James Ross, Epica Dronning Maud Land, Vostok, Taldice, Law Dome), a proxy of annual mean temperature, and the associated EOF pattern. Numbers on the maps represent the correlation coefficient of each $\delta^{18}O$ record with PC1 (upper map) and PC2 (lower map). Positive correlations are noted in red colours while negative correlations are noted in blue colours. (For interpretation of the references to colour in this figure legend, the reader is referred to the web version of this article.)

as a proxy for regional recession of marine-based glaciers and ice shelves via iceberg and brash ice discharge and/or frontal and basal melting. We assume that ablation rates of advancing glaciers are too small to significantly and durably affect the $\delta^{18}O_{diatom}$ signal. We first describe the variations in glacial ice melt over the Holocene and, second, detail the respective role of atmospheric and oceanic processes by confronting the records of (1) past surface air temperature records and sea-surface temperatures and sea-ice records and (2) transient simulations of air and ocean temperatures from the IPSL-CM5A-LR coupled model.

4.1. Holocene glacial discharge around Antarctica

In core JPC24, the $\delta^{18}O_{diatom}$ values vary between 41.9‰ and 45.5‰ (Fig. 3A). This range is in agreement with previously published records from AL (Fig. 3B) (Crespin et al., 2014) and the Atlantic sector of the SO (Shemesh et al., 1995, 2002). It is also close to the range observed in the WAP (Fig. 3C) (Pike et al., 2013).

In core JPC24, the $\delta^{18}O_{diatom}$ values increase from ~9 kyr BP to ~5 kyr BP and subsequently decrease until the core-top (Fig. 3A). The decrease is especially pronounced over the last ~3.5 kyr. Centennial events are present over the Holocene with low values evidenced at ~8.8 kyr BP, ~6.3 kyr BP, ~5.8 kyr BP, ~4.2 kyr BP, ~3–2.3 kyr BP and ~1.9–0.9 kyr BP. In comparison, the $\delta^{18}O_{diatom}$ values in core MD03–2601 from AL are rather stable over the ~9–4 kyr BP time interval before declining until 1 kyr BP (Fig. 3B) as similarly illustrated in the new PB record. Centennial variability roams the record with particularly low values observed at ~7–6 kyr BP, ~4 kyr BP, ~3–2.5 kyr BP and ~1.8 kyr BP. Interestingly, the $\delta^{18}O_{diatom}$ record in the ODP site 1098 from the WAP shares a pattern very similar to the one observed in core JPC24 with an increasing trend until ~4 kyr BP and a subsequent decrease until sub-recent times (Fig. 3C). The decrease becomes steeper after 2 kyr BP as observed for the other $\delta^{18}O_{diatom}$ records. Lowest values at the centennial scale are observed during the early Holocene at ~9–8 kyr BP, ~4.3 kyr BP and since 2.5 kyr BP.

The three $\delta^{18}O_{diatom}$ records suggest a similar long-term behaviour of glacial systems around Antarctica. Taken together, they suggest high glacial ice discharge and/or melt during the 9–8 kyr BP time interval. This period represents the terminal phase of the last deglaciation in East Antarctica (Ingólfsson et al., 1998; Mackinstosh et al., 2014) and northwestern Antarctic Peninsula (Ingólfsson et al., 1998; Heroy and Anderson, 2007; O'Cofaigh et al., 2014). Glacial discharge was then reduced during the 8–4.5 kyr BP time interval when the Antarctic ice sheet stabilized (O'Cofaigh et al., 2014). A glacial readvance during the ~6–4 kyr BP period is even inferred for the Antarctic Peninsula, Vestfold Hills and Bunger Hills nearby PB and East Antarctica (Ingólfsson et al., 1998). However, the $\delta^{18}O_{diatom}$ record in core MD03–2601 suggests that some local glaciers off Wilkes Land may have retreated during the 7–6 kyr BP period (Fig. 3C). Glacial discharge increased again, and was more variable, since 4.5 kyr BP possibly due to glacier oscillations (Ingólfsson et al., 1998; O'Cofaigh et al., 2014). In PB, micropaleontological and sedimentological studies inferred a continuous thinning and recession of the Amery Ice Shelf since 5.7 ^{14}C kyrs BP (Hemer and Harris, 2003; Hemer et al., 2007). The coherent multimillennial pattern of enhanced glacial discharge since ~4.5 kyr BP, from three different regions around Antarctica argue for common driving mechanisms. However regional discrepancies at the centennial timescale, due to local response of the cryospheric system, may have existed.

4.2. Atmospheric driving mechanisms

4.2.1. Air temperature trends from ice core records

Atmospheric warming has been shown to enhance glacier thinning and recession over the past ~40 years (Miles et al., 2013) and snow melt in Antarctic Peninsula over the 20th century (Abram et al., 2013). Building on this, previous studies on $\delta^{18}O_{diatom}$ proposed that atmospheric warming, due to increasing amplitude of ENSO variability and dominance of La Niña over El Niño, drove marine terminating glacier melting and calving in Antarctic Peninsula (Pike et al., 2013) and Wilkes Land (Crespin et al., 2014) over the past 4 kyr. We here compiled $\delta^{18}O$ records from Antarctic ice cores and use transient simulations to test whether surface air temperatures (SAT) variations over Antarctica and the SO provide a robust forcing to glacial discharges. We then use the 20CR historical reanalysis over the 1870–2010 period (Compo et al., 2011) to determine the climatic impact of ENSO over the three regions were $\delta^{18}O_{diatom}$ records exist along with transient simulations to compute the number of El Niño and La Niña events over the 6–4 kyr BP, 4–2 kyr BP and 2–0 kyr BP periods.

Common signals were extracted using principal component analysis from the 200-year resampled $\delta^{18}O$ records of ten ice cores (Fig. 4). The first two Empirical orthogonal function (EOF) together explain 80% of the data variance. More than one half (52%) of the variance is captured by the first EOF, whose principal component (PC1) is showing a decreasing trend from 9 to 1 kyr BP. PC1 is positively correlated to Dome F, James Ross, Vostok and Law Dome records, while negatively

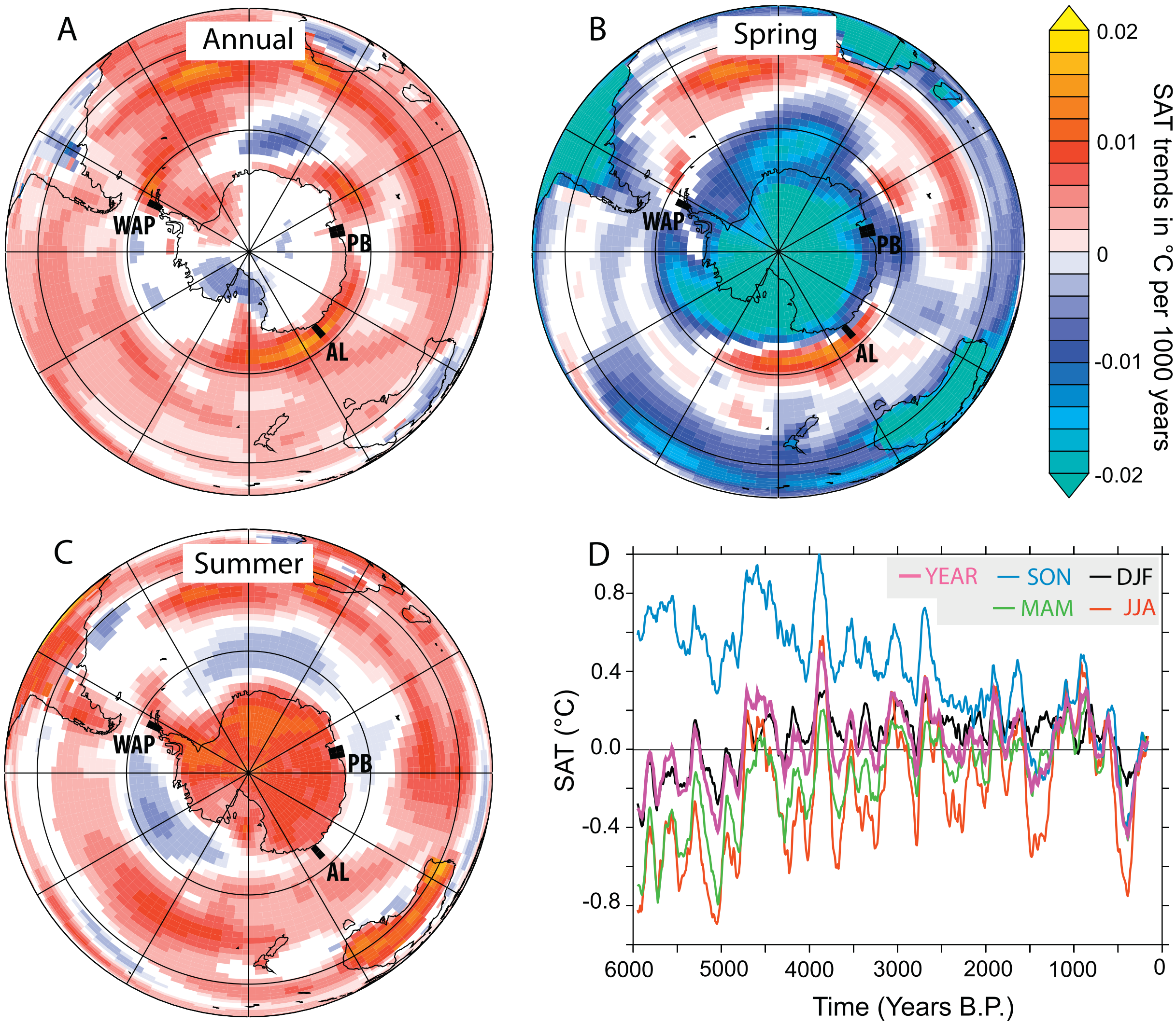

Fig. 5. Maps of simulated surface air temperature (SAT, in °C) trends in the mean of the three-member ensemble over the period 6–0 kyr BP. A) Annual mean, B) Austral spring (SON) and C) Austral summer (DJF). Regressions are in 0.01 °C per thousand years. D) Time series of the ensemble mean SAT south of 60°S, with the annual mean value in pink, the Austral winter (average of June–July–August, JJA) in red, the Austral summer (average of December–January-February, DJF) in black, the Austral spring (average of September–October–November, SON) in blue, the Austral autumn (average of March–April–May MAM) in green. WAP: Western Antarctic Peninsula; PB: Prydz Bay; AL: Adélie Land. (For interpretation of the references to colour in this figure legend, the reader is referred to the web version of this article.)

correlated to Byrd, Siple, WAIS, TALDICE and EDC records. This spatial distribution stresses a dipole-pattern between the Atlantic-Indian, where the Holocene is dominated by a cooling trend, and the Pacific sectors of Antarctica, where a warming trend is observed, somehow similar to modern ENSO teleconnection pattern at high southern latitudes (Turner, 2004; Yuan, 2004; Dash et al., 2013). PC2, associated with EOF2 (28% of the total variance), shows an increase from ~7.5 kyr BP to ~4.5 kyr BP and a subsequent continuous decrease until modern time. It is positively correlated with James Ross, WAIS, EDML TALDICE and EDC records, where a cooling trend is inferred over the past ~4.5 kyr, and negatively correlated with Siple where a late Holocene warming trend is observed. Both PC1 and PC2 also show millennial variability as already evidenced in a previous EOF analysis (Masson et al., 2000). Our new analysis, based on better resolved and more numerous Holocene $\delta^{18}O$ records, demonstrates that East Antarctica and the Antarctic Peninsula experienced a cooling trend over the past ~4.5 kyr (Fig. 4) when the marine $\delta^{18}O_{diatom}$ records suggest increasing glacial ice discharge and/or melt (Fig. 3A–C). The conversion of $\delta^{18}O$ data from Vostok, EDML, Dome F, Law Dome and JRI, that present a significant positive correlation on EOF 1 or 2, or both, without showing a significant negative trend on the other EOF, in air temperature over Antarctica using the latest regional $\delta^{18}O$-temperature relationships (Stenni et al., 2017) reconstructs a mean cooling of ~2.5 °C over the last 4 kyr. Only the eastern Ross Sea region experienced a robust warming whereby both Siple and Byrd sites are negatively correlated to PC1 and PC2 decreasing trends. The conversion of their $\delta^{18}O$ data indicates a mean regional warming of ~1.9 °C over the past 4 kyr. Conversely, the nearby WAIS record along with EDC and TALDICE reveal an ambiguous Holocene $\delta^{18}O$ trend with significantly negative values on EOF 1 (warming) and a significant positive value on EOF 2 (cooling). These sites however experienced a mean cooling of ~1 °C over the past 4 kyr. As such, ice core data suggest a general cooling over most of Antarctica, especially pronounced during the Late Holocene (Fig. 4), which cannot explain the observed greater glacial ice discharge and/or melt since 4 kyr BP. The late Holocene cooling trend may have however promoted glacier advance allowing more ice to be in contact with the surrounding ocean, which subsequent retreat would have lowered the $\delta^{18}O_{seawater}$ and thence the $\delta^{18}O_{diatom}$ values.

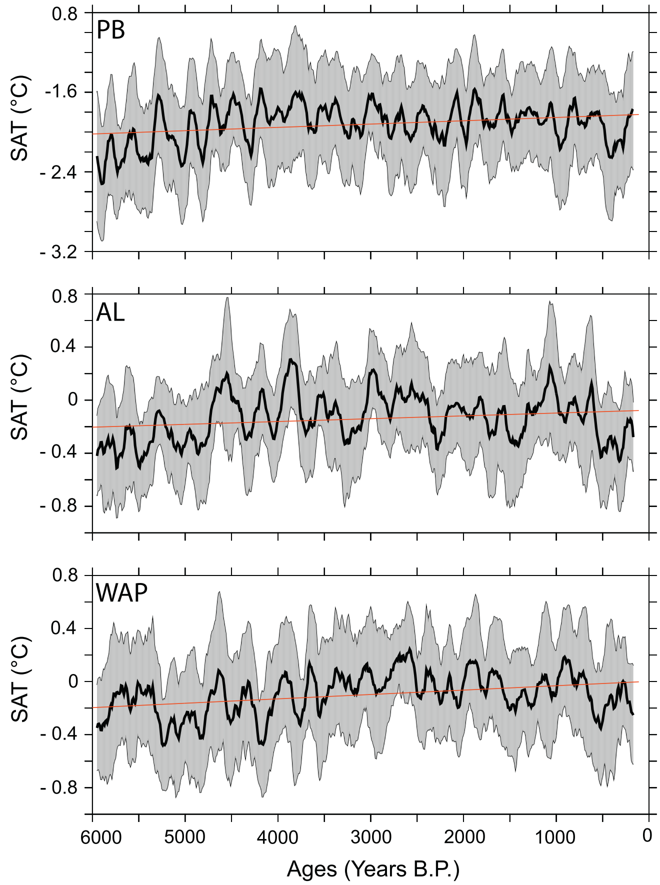

Fig. 6. Simulated summer (DJF) surface air temperature (SAT) in the mean of the three-member ensemble at the three cores locations over the period 6–0 kyr. The grey shading represents one standard deviation among the three members and the black line the ensemble mean. The red line is a linear regression of the ensemble mean. PB: Prydz Bay; AL: Adélie Land; PD: Palmer Deep. (For interpretation of the references to colour in this figure legend, the reader is referred to the web version of this article.)

4.2.2. Air temperature trends from transient climate simulations

To further document and understand the mechanism behind the annual and seasonal trends in SAT over Antarctica and the SO, we use simulations from the IPSL-CM5A-LR model (Dufresne et al., 2013) integrated over 600 years with an insolation forcing accelerated by 10, therefore covering the last 6 kyr. The mean of the 3-member ensemble shows weak, but significant at the 95% level using a *t*-test, negative annual mean SAT trends over the Antarctic continent (Fig. 5A). The trends appear more pronounced around the Ross Sea region. The simulated trends are generally coherent with the PC1 from ice core $\delta^{18}O$ records (Fig. 4), except for the eastern Ross Sea region where ice core records infer a robust warming trend over the Late Holocene. These annual trends result from opposite seasonal trends (Fig. 5B–D). South of 60°S, warming trends are simulated for all seasons except for spring that is characterised by strong cooling trends during the last 6 kyr (Fig. 5B). More precisely, the mean spring SAT integrated between 60 and 90°S is simulated to decrease by ~0.80 °C during the last 6 kyr while the autumn and winter SAT concomitantly increased by ~0.80 °C (Fig. 5D). Over the same period, summer SAT is simulated to increase by ~0.4 °C. Both spring SAT decrease and summer SAT increase are continent wide (Fig. 5B, C). These trends seemingly reflect linearly the distribution of seasonal insolation at very high southern latitudes with spring insolation decreasing by ~30 $W{\cdot}m^{-2}$ while summer insolation increased by 15 $W{\cdot}m^{-2}$ over the last 6 kyr (Fig. 2).

We then extracted the mean summer SAT from the 3-member ensemble over the period 6–0 kyr BP at each marine core site (Fig. 6). Modelled summer SAT for the most recent times are in good agreement with modern mean summer SAT recorded in PB (−1 °C in January but −4 °C in February at Davis Station; http://www.bom.gov.au), AL (−1 °C in December–January; König-Langlo et al., 1998) and WAP (1–2 °C in December to February at Faraday/Vernadsky Station, Franzke, 2013). Coastal air temperatures can however get episodically positive during summer under very specific atmospheric conditions such as foenh winds in Eastern Antarctic Peninsula (Cape et al., 2015) or warm air masses mixing by katabatic winds in East Antarctica (Lenaerts et al., 2016). Both our model simulations and geological data cannot however track such rapid events, generally lasting few days, whose repetition can enhance surface melt. Small, but significant (*t*-test, 95% level) positive summer SAT trends are simulated at each marine core site over the last 6 kyr (Fig. 6). These trends are however very small, reaching ~0.2 °C in PB and the WAP and ~0.1 °C in AL in 6000 years and thus not strong enough to induce strong changes in summer surface melting. Additionally, these linear trends mask small SAT decreases since 3–2.5 kyr BP in AL and WAP, in agreement with the general cooling over East Antarctica and the Antarctic Peninsula suggested by the ice core data.

4.2.3. Relationship with ENSO

Ice core data show a SAT decreasing trend during the late Holocene while model simulations suggest a concomitant small increase in SAT. These changes in atmospheric temperature cannot explain the inferred increase in glacial ice discharge/melt over the Late Holocene, therefore casting doubt on previous interpretations suggesting a causal relationship between ENSO and melting of marine-terminating glacier (Pike et al., 2013; Crespin et al., 2014). Indeed, Pike et al. (2013) related their low $\delta^{18}O_{diatom}$ data recorded at Palmer Deep during the late Holocene to enhanced glacial ice discharge. The main cause of such enhanced glacial discharge would have been a regional atmospheric warming and an increase in moisture delivery in response to (i) greater ENSO frequency from ~2.2 kyr BP (Moy et al., 2002; Conroy et al., 2008) and (ii) increased La Niña intensity (Makou et al., 2010) as well as (iii) peak summer insolation at 60°S (Berger and Loutre, 1991). However, no link between high ENSO activity and low $\delta^{18}O_{diatom}$ values is observed during other periods of the Holocene. Indeed, a new reconstruction from Galapagos Islands inferred high ENSO activity between 9 and 5.5 kyr BP (Zhang et al., 2014), congruent to an increase towards heavier $\delta^{18}O_{diatom}$ values (Fig. 3A,C) indicating less glacial melting both in WAP and East Antarctica. In order to test the hypothesis of ENSO-related atmospheric warming of Antarctica since 4 kyr BP, we first investigated the current low to high-latitudes teleconnections by producing a composite map of SAT using HadISST data over the 1870–2010 period with Niño3.4 index (Fig. 7). We then computed the number of El Niño and La Niña events over the 6–4 kyr BP, 4–2 kyr BP and 2–0 kyr BP periods in the three-member ensemble.

Composite analysis of standard El Niño events (Fig. 7A) indicates a weak cooling in PB and WAP and no significant SAT changes in AL. Comparatively, standard La Niña conditions lead to a weak warming in PB and WAP and no significant SAT changes in AL (Fig. 7B). Only extreme El Niño events induce significant SAT changes in Antarctica with a > 1 °C SAT decrease in PB and WAP along with 0.5 °C SAT increase in AL (Fig. 7C). During extreme La Niña events, similar amplitude SAT changes of opposite signs are observed at the three core sites (Fig. 7D). The > 1 °C warming induced by La Niña in PB and WAP, and El Niño in AL, is however not sufficient for SAT to reach positive values in PB and AL whereby summer SAT is around −1 °C in these regions (König-Langlo et al., 1998). Strong and sustained El Niño events may induce surface melt in very sensitive regions of West Antarctica (Nicolas et al., 2017). However, the predominance of La Niña over El Niño as the main forcing mechanism of WAP glacial discharge during the Late Holocene (Pike et al., 2013) would have conducted to a coastal cooling in AL, at odds with the $\delta^{18}O_{diatom}$-inferred circum-Antarctic increase in glacial discharge over the last 4 kyr (Figs. 3A–C, Fig. 8).

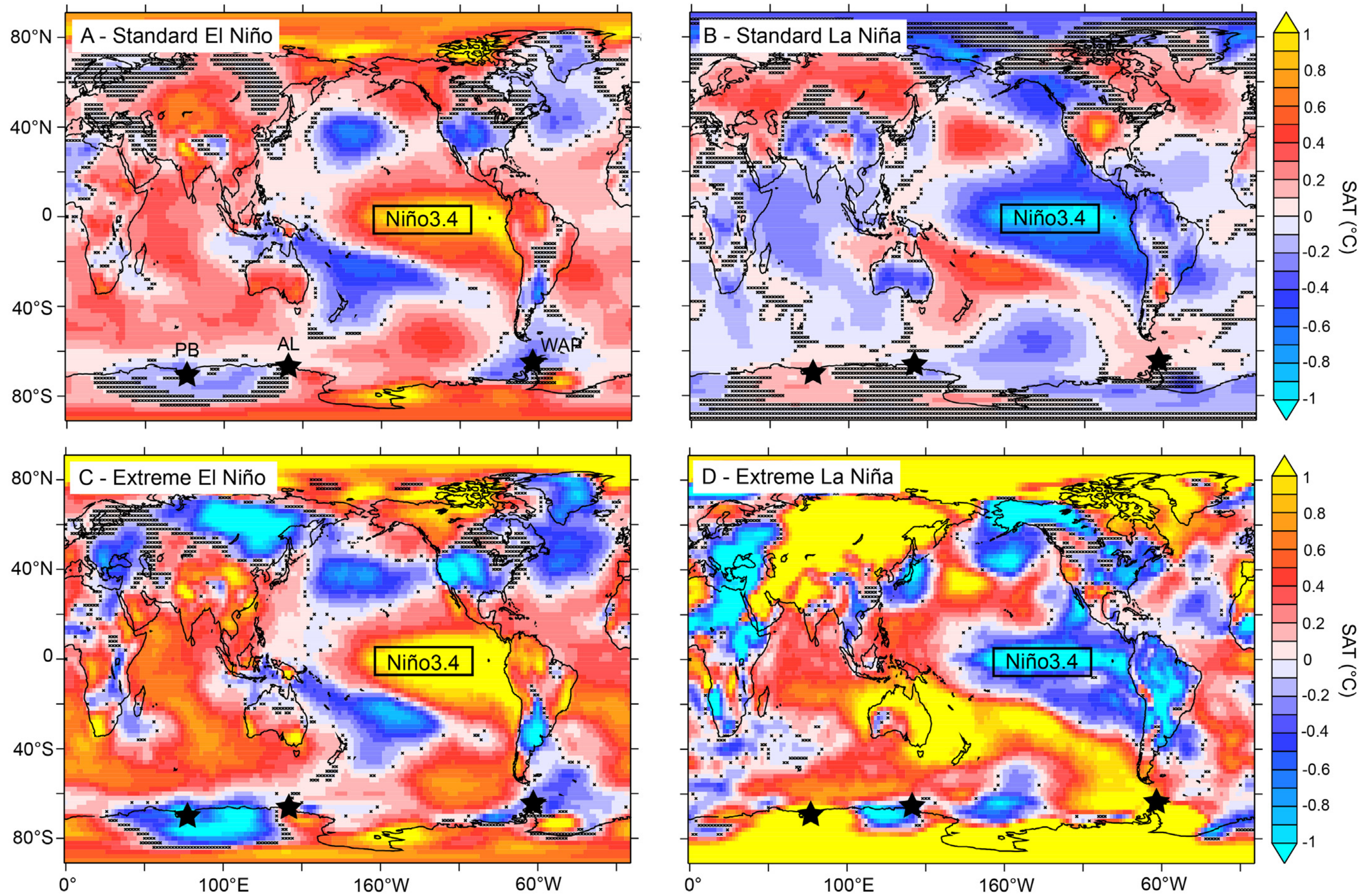

Fig. 7. Composite map of surface air temperature (NOAA-20CR reanalysis; Compo et al., 2011) in Austral spring (SON, the main season of analyzed proxies) on Niño3.4 index using HadISST data (Rayner et al., 2003) over the 1870–2010 period. A: Composite for El Niño events larger than 1 standard deviation of the Niño3.4 box (hereafter called standard El Niño, 26 events); B: Composite for La Niña events lower than 1 standard deviation of the Niño3.4 box (hereafter called standard La Niña, 26 events); C: Composite for extreme El Niño events larger than two standard deviations of the Niño3.4 box (hereafter called extreme El Niño, 5 events); D: Composite for extreme La Niña events lower than two standard deviations of the Niño3.4 box (hereafter called extreme La Niña, 1 event). The main patterns found remains similar for annual means instead of Austral spring.

We also explored the recurrence and amplitude changes of ENSO through mean simulated SST in the Nino3.4 box in the three-member ensemble (Fig. 8). The different simulations do not show any significant changes in ENSO amplitude and frequency in three different time slices of 2000 years (e.g. 200 accelerated years). Indeed, there are no significant changes in phase dominance with comparable numbers of El Niño and La Niña (around 30 each) during the 6–4 kyr BP, 4–2 kyr BP and 2–0 kyr BP periods.

Although a recent study suggests that the current generation of coupled climate model may not adequately simulate ENSO response to astronomical forcing (Emile-Geay et al., 2015), our ensemble-mean simulations do not show large changes in ENSO variability during the Holocene and therefore question the possibility of a dominant role of ENSO, via atmospheric Antarctic warming, on glacier and ice shelves melting/calving during the Late Holocene. Additionally, geological data deliver a blurry picture of ENSO activity during the Holocene. Lacustrine records from Ecuador (Moy et al., 2002) and mid-Equatorial Pacific (Conroy et al., 2008) indicate strong ENSO intensity and frequency during the past 4 kyr, although a more recent study also from Galapagos Islands suggests that El Niño activity was more moderate during this period and not different than during the early-mid Holocene (Zhang et al., 2014). Coral records from the Equatorial Pacific conversely suggest no systematic trends in ENSO variance over the last 7 kyr (Cobb et al., 2013). In conclusion, given the results from model simulations and the erratic information delivered by geological records, ENSO intensification during the Late Holocene and associated enhanced impact on high surface air temperatures remains questionable.

4.3. Oceanic forcing

As atmospheric temperature changes cannot explain the late Holocene increase in glacial discharge recorded in three different locations around Antarctica, we subsequently compared the $\delta^{18}O_{diatom}$ records to sea-ice and SST records at the three core sites and present transient simulations of SO water temperature evolution to test whether change in ocean thermal content could have driven the inferred greater glacial discharge over the last 4 kyr.

4.3.1. Information from regional paleoceanographic records

Sea-ice changes over the Holocene are estimated from the relative abundances of the *Fragilariopsis curta* diatom group (*F. curta* gp; Gersonde and Zielinski, 2000). In Antarctic coastal areas, higher values of the *F. curta* gp track longer sea-ice duration in spring/summer (Campagne et al., 2016). The *F. curta* gp records demonstrate greater sea-ice cover at the three core sites since ~4 kyr BP (Fig. 3D–F) although differences exist in the exact timing and amplitude of the increase between the proxies and sites. These interpretations are in agreement with the simulated Holocene long-term increase in spring sea-ice concentration and thickness (Renssen et al., 2005).

At the core locations, subsurface temperature changes over the Holocene are estimated from the TEX_{86}^{L} (TetraEther Index of tetraethers with 86 carbons) (Kim et al., 2010). In Antarctic coastal areas,

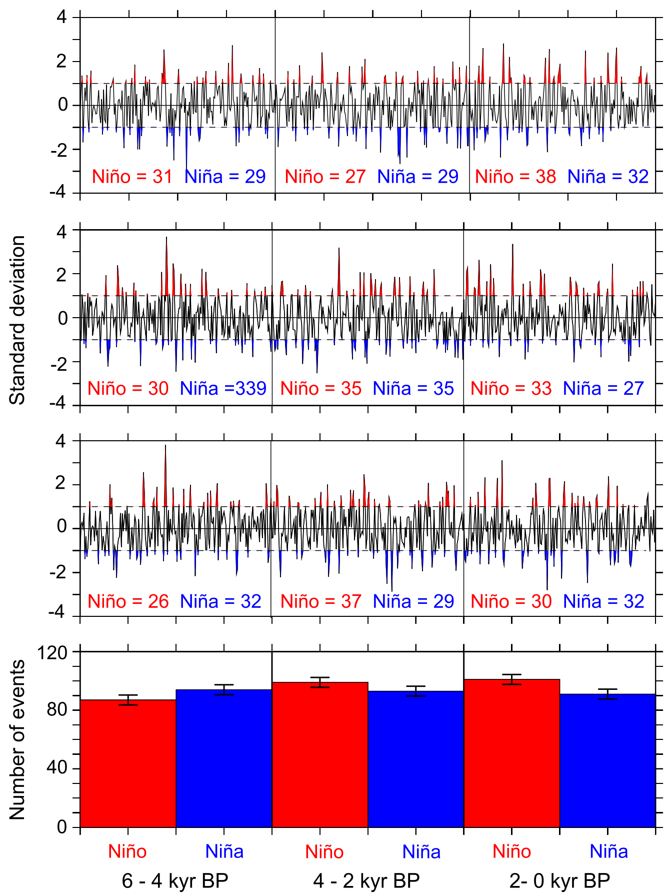

Fig. 8. Evolution of SST in Niño3.4 box in the three simulations of the three-member ensemble. For each 200-year period (corresponding to changes in insolation of 2000 years), we computed the number of Niño and Niña events defined as events larger than one standard deviation. The last panel show the total number of events in the three different simulations for El Niño events in red and La Niña events in blue. The error bar represents one standard deviation computed over the whole simulations available. None of the differences between the periods are statistically significant at the 95% level using a student test. (For interpretation of the references to colour in this figure legend, the reader is referred to the web version of this article.)

this proxy tracks annual temperatures integrated over the 0–200 m water depth (Etourneau et al., 2013) and is influenced by the mCDW. Records from WAP and AL both show no overall trends over the past 9 kyr but evidence enhanced variability since ~2.5 kyr BP, with warmings up to 4 °C in amplitude (Fig. 3G–H), interpreted as episodic intensification of CDW intrusion over the Antarctic coastal shelf (Shevenell et al., 2011; Kim et al., 2012; Etourneau et al., 2013). No subsurface temperature record exists at JPC24 core site in PB. However, increasing relative abundances of the setae diatom group since ~6 kyr BP in core JPC24 were suggested to indicate enhanced water column mixing and CDW intrusion into PB (Denis et al., 2010). We speculate that episodic warming of subsurface waters during the late Holocene may thus have contributed to the frontal and basal melting of marine-based glaciers and ice shelves, as observed today (Rignot et al., 2013; Miles et al., 2013). Indeed, a recent study, based on an advanced two-dimensional meltwater plume model, showed that a 0.8 °C ocean warming induces a basal melting of ~0.3 m·yr^{-1} (Ross Ice Shelf) and up to ~4 m·yr^{-1} in (Filchner-Ronne Ice Shelf) depending on the local bathymetry and the geometry of the ice shelves (Lazeroms et al., 2018). Additionally, Holland et al. (2008) showed that basal melt rates obtained from a general ocean circulation model respond quadratically to changing ocean temperatures. We therefore suggest that repeated events of SOT warming > 1 °C observed during the Late Holocene had a strong impact on basal melting and ice shelves destabilization.

4.3.2. Subsurface SO temperatures in transient simulations

Increased spring sea-ice cover and duration in coastal Antarctica (PB, AL and WAP) during the last 4 kyr appears at odds with repeated subsurface warming events (Fig. 3). Changes in sea-ice seasonality over the Holocene was already suggested with early spring melting but early autumn freezing during the Mid-Holocene Hypsithermal and late spring melting but late autumn freezing during the Late Holocene Neoglacial (Pike et al., 2009). Changes in seasonal insolation south of 60°S were suggested to be the main forcing mechanism whereby the strong decrease in spring insolation over the last 6 kyr (~30 W·m^{-2}; Fig. 2) would have allowed spring sea ice to melt later in the year while the increase in summer insolation (~15 W·m^{-2}) would have allowed ice free surface water to warm and delay autumn sea-ice formation (Pike et al., 2009). Our simulations confirm that changes in seasonal insolation had a profound impact on surface and subsurface ocean temperatures which, in turn, may have impacted on glacial ice discharge.

The simulated Holocene response of summer subsurface temperature in the three-member ensemble shows an increase in the 0–200 m water depth since ~5 kyr BP, with episodic warm anomalies reaching down to 500 m during the 5–2 kyr BP period (Fig. 9A). This warming can be interpreted as a direct response to the increase in summer insolation south of 60°S (Fig. 2) which is penetrating at depth. The seasonal deepening of the mixed layer through time may then explain the thickening of the simulated warm surface-subsurface layer down to ~300 m during the autumn (Fig. 9B). The warm anomaly, initiated in summer, is then stored below the sea-ice lid, essentially in the upper 100–150 m, during the following winter and spring (Fig. 9C–D). Greater sea-ice cover in spring insulates the ocean from the atmosphere, thus limiting the impact of the negative trend in spring insolation and the loss of the warm anomaly initiated the previous summer. The warm summer anomaly, stored in subsurface waters, would have then promoted melting of marine-terminating glaciers and ice-shelves. We note that global circulation models present large uncertainties in the SO and are known to under-estimate seasonal and long-term changes in the depth of the mixed layer and the wind stress field (e.g. Dufresne et al., 2013).

Water masses involved in marine-terminating glaciers and ice-shelves melting are generally in the 200–800 m depth range and originate from the intrusion of CDW onto the Antarctic continental shelf via troughs and channels (Foldvik et al., 2004; Herraiz-Borreguero et al., 2015; Liu et al., 2017; Nitsche et al., 2017; Walker and Gardner, 2017). The CDW upwells mostly along the southern boundary of the ACC (Tamsitt et al., 2017), which is closest to the Antarctic continent in Prydz Bay, Adélie Land and western Antarctic Peninsula (Orsi et al., 1995), facilitating the penetration of CDW onto the shelf in these regions. Our transient simulations demonstrate a warming of the CDW at 2 kyr BP compared to 6 kyr BP (Fig. 10, red-yellow shading). A positive anomaly of > 0.25 °C is simulated over the upper 500 m in the upwelling zone and is transported southward until the Antarctic coast where it thickens to ~1000 m allowing for the intrusion of warmer water in subice cavities where it can interact with ice-shelves and marine-terminating glaciers.

4.3.3. Driving mechanisms for late Holocene glacial discharge-melt

The SO overturning circulation is enhanced at 2 kyr BP (Fig. 10, green line) compared to 6 kyr BP (black line) and is displaced southward. This effect is also capable of facilitating intrusion of CDW onto the Antarctic continental shelf. The upwelling is located at 40–50°S in the model, which is ~10° of latitude northward of its modern day in situ location. Thus intrusion of the warm anomaly may have been even more intense than modelled here. This slightly more intense and southward located upwelling at 2 kyr BP compared to 6 kyr BP may respond to the southward migration of the Southern Hemisphere Westerlies winds (SWW). Indeed, our simulations demonstrate a

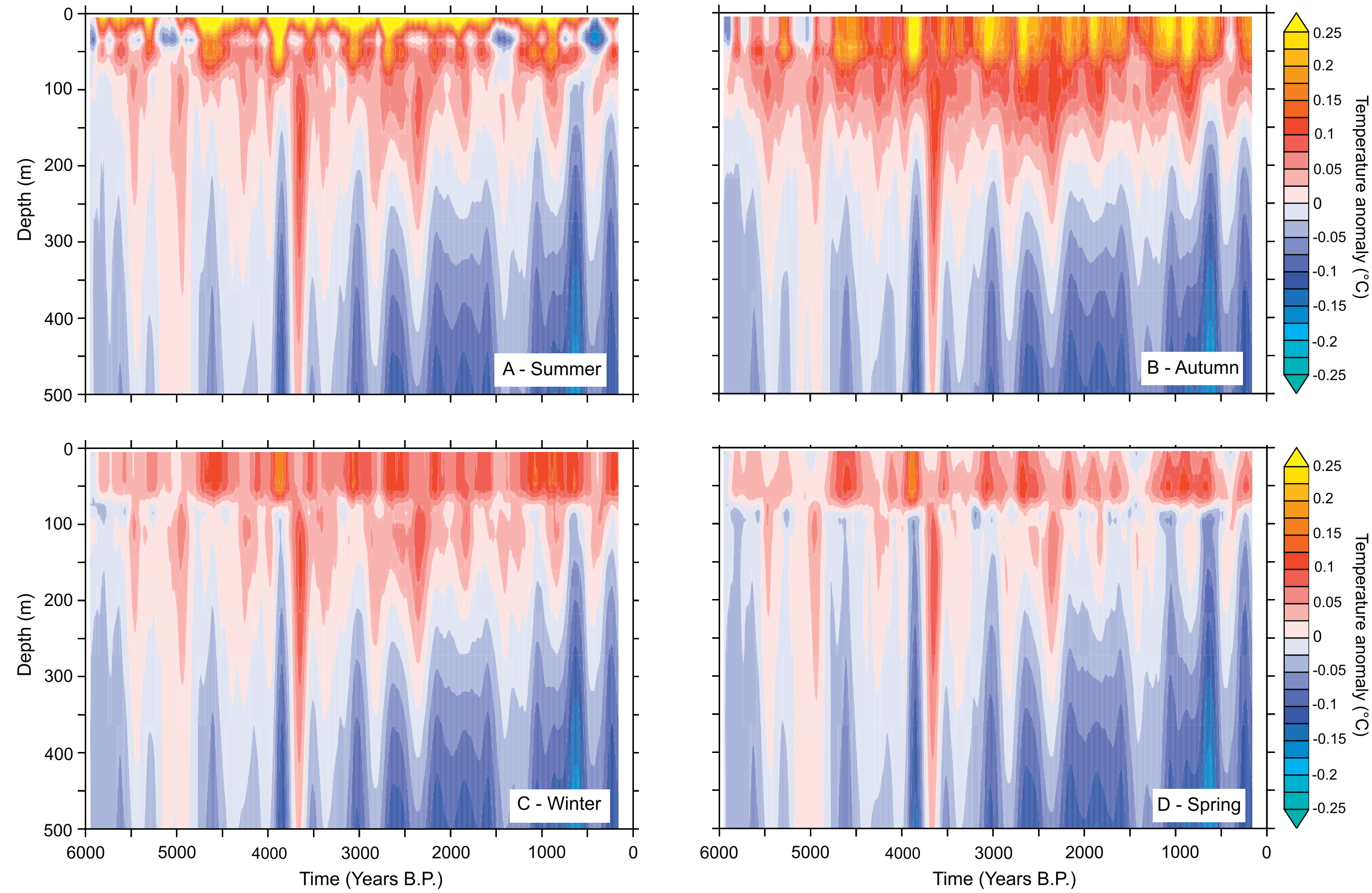

Fig. 9. Simulated seasonal ocean temperature anomalies (reference period is the first 10 years of the simulation starting at 6 kyr BP) averaged south of 60°S for the first 500 m in the mean of the 3-member ensemble over the period 6–0 kyr BP.

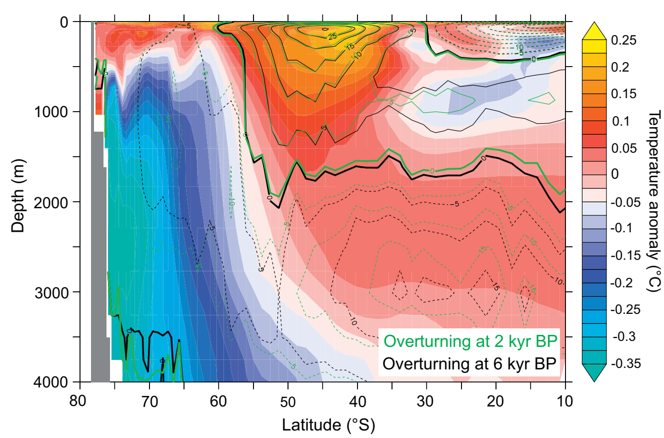

Fig. 10. Simulated annual mean ocean temperature anomalies (in °C) between 2 kyr BP and 6 kyr BP over the global ocean south of 10°S for the first 4000 m in the 3-member ensemble mean along with the simulated meridional overturning circulation function at 2 kyr BP (green) and 6 kyr BP (black) (in sverdrups). Reddish colours indicate a warming between 6 kyr BP and 2 kyr BP while blueish colours indicate a cooling over the same period. The intensification and southward migration of the SO upwelling during the Late Holocene is identified by the greater, slightly poleward displaced, streamfunction values at 2 kyr BP (green line) than at 6 kyr (black line). (For interpretation of the references to colour in this figure legend, the reader is referred to the web version of this article.)

deepening of the Antarctic Circumpolar Trough during the Holocene (Fig. 11), conducting to a strengthening and poleward displacement of the SWW as already observed in intermediate complexity models (Renssen et al., 2005; Varma et al., 2012). Geological data similarly suggest a southernmost position of the SWW during the ~6–2 kyr BP period (Voigt et al., 2016), a southward migration of the maximum surface wind speed over the Holocene (Voigt et al., 2015) and an intensification of the core SWW since ~5 kyr BP (Lamy et al., 2010). Enhanced and poleward displaced SWW increase the penetration of NADW at depths and of warmer waters of subtropical origin at surface into the SO (Delworth and Zeng, 2008). Both processes warm the CDW. Poleward displaced SWW probably pushed the southern ACC further to the south thus increasing CDW resurgence onto the Antarctic continental shelf.

We thus suggest that both changes in seasonal insolation and SO overturning circulation acted synergistically to warm subsurface and deep waters which interacted with marine-terminating glaciers and ice-shelves over the past 4 kyr. The increased glacial ice discharged reduced sea-surface salinity, as shown by the lower $\delta^{18}O_{diatom}$ values since ~4 kyr BP, facilitating sea-ice formation during winter and sea-ice persistence during spring (Bintanja et al., 2013), thus providing a positive feedback on Holocene long-term increasing seasonality. The cooling of deep and bottom waters between 1000 m and 4000 m produced at the Antarctic slope in our transient simulation (Fig. 10, blue shading) may result from the greater seasonal sea-ice cycle observed in geological records (Fig. 3; Pike et al., 2009). More sea-ice formation in winter induces, in the IPSL model, a stronger convection transporting down colder and denser waters. This greater downwelling could have been compensated, through volume conservation, by a greater SO upwelling, providing an additional mechanism for the intrusion of CDW

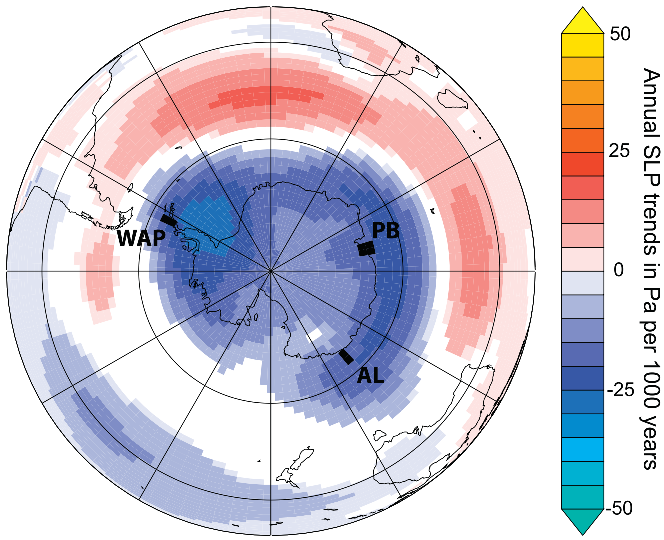

Fig. 11. Trends of simulated annual mean sea level pressure (Pa/1000 yr) for the mean of the 3-member ensemble over the period 6–0 kyrs BP.

onto the Antarctic continental shelf (Fig. 10). If so, CDW intrusion onto the shelf may have peaked in winter (Liu et al., 2017) when sea ice insulates the ocean from the atmosphere, thus reducing heat content loss to the atmosphere.

5. Conclusions

A new Holocene $\delta^{18}O_{diatom}$ record from Prydz Bay has been combined to previously published records from Adélie Land and western Antarctic Peninsula. All three records indicate an increase in glacial ice discharge and/or melt since ~4 kyr BP. Similar signals argue for a common driving mechanism.

Using ice core data we demonstrate a general atmospheric cooling over Antarctica since ~4.5 kyr BP that cannot be reconciled with enhanced glacial discharge and/or melt. Using a three-member ensemble of new transient accelerated simulations from the IPSL-CM5A-LR coupled model from 6 kyr BP to present days, we show that an atmospheric warming might have occurred in summer, in response to an increase in local summer insolation, but is too small to have induced significant changes in surface melting over Antarctica. Finally, using historical observations and reanalysis, we show that ENSO-driven atmospheric teleconnections, that imply strong spatial climate heterogeneities in Antarctica, cannot explain similar $\delta^{18}O_{diatom}$ records.

Conversely, our new transient simulations suggest a long-term increase in annual subsurface and deep oceanic temperatures. The modelled subsurface warming agrees reasonably well with geological records from Adélie Land and western Antarctic Peninsula, whereby greater variability in TEX_{86}^{L}-based subsurface temperature is reconstructed over the late Holocene. The subsurface warming appears to be a response to increasing summer insolation at very high southern latitudes whose signal at depth might be preserved through insulation effect by the sea-ice cover, most notably in winter and spring. The deep warming is probably associated with the simulated intensification and southward migration of the SO upwelling in response to the deepening of the Circumpolar Trough and southward migration and intensification of the southern westerly winds over the Holocene. The magnitude of the oceanic warming is large enough to have a strong impact on glaciers and ice shelves melting.

Finally, we propose a new scenario reconciling the observed long-term changes in sea-ice seasonality over the Holocene whereby the Late Holocene experienced heavier coastal sea-ice duration in spring but warmer surface and subsurface waters in summer compared to the Mid-Holocene. Heavier sea-ice conditions may result from decreasing high-latitude spring insolation and lower surface salinity due to glacial ice discharge and/or melt while higher summer surface and subsurface may result from increasing high-latitude summer insolation and more intense upwelling of CDW.

Acknowledgments

We thank Amy Leventer, Eugene Domack and Rob Dunbar for giving access to core NBP0101-JPC24 retrieved during the NSF funded CHAOS oceanographic cruise. The research leading to this study was partially supported by The De Botton Center for Marine Sciences at the Weizmann Institute and a Feinberg Graduate School post-doctoral fellowship from the Weizmann Institute to J.C. This research has also received funding from the French National Research Agency HAMOC project (Grant ANR-13-BS06-0003) and the ESF PolarClimate HOLOCLIP Project (Polar-FP-625). C.X. and D.S. are funded by CNRS-INSU. V.M.-D. acknowledges support from ANR ASUMA (grant ANR-14-CE01-0001). H.G. is Research Director with the F.R.S-FNRS, Belgium. This is a HOLOCLIP publication number 31.

References

Abelmann, A., Gersonde, R., Knorr, G., Zhang, X., Chapligin, B., Maier, E., Esper, O., Friedrichsen, H., Lohmann, G., Meyer, H., Tiedemann, R., 2015. The seasonal sea-ice zone in the glacial Southern Ocean as a carbon sink. Nat. Commun. 6, 8136. http://dx.doi.org/10.1038/ncomms9136.

Abram, N.J., Mulvaney, R., Wolff, E.W., Triest, J., Kipfstuhl, S., Trusel, L.D., Vimeux, F., Fleet, L., Arrowsmith, C., 2013. Acceleration of snow melt in an Antarctic Peninsula core during the twentieth century. Nat. Geosci. 6, 404–411.

Abram, N.V., McGregor, H.V., Tierney, J.E., Evans, M.N., McKay, N.P., Kaufman, D.F., the PAGES 2k Consortium, 2016. Early onset of industrial-era warming across the oceans and continents. Nature 536, 411–418.

Allen, C.S., Oakes-Fretwell, L., Anderson, J.B., Hodgson, D.A., 2010. A record of Holocene glacial and oceanographic variability in Neny Fjord, Antarctic Peninsula. The Holocene 20 (4), 551–564.

Bakker, P., Clark, P.U., Golledge, R.N., Schmittner, A., Weber, N.E., 2017. Centennial-scale Holocene climate variations amplified by Antarctic ice sheet discharge. Nature 541, 72–76.

Barbara, L., Crosta, X., Massé, G., Ther, O., 2010. Deglacial environments in eastern Prydz Bay, East Antarctica. Quat. Sci. Rev. 29, 2731–2740.

Barnes, D., Bergstrom, D., Bindschadler, R., Bockheim, J., Bodeker, G., Bopp, L., Bracegirdle, T., Chown, S., Convey, P., di Prisco, G., Fahrbach, E., Forcada, J., Frenot, Y., Goosse, H., Gutt, J., Hodgson, D., Huiskes, A., Jones, A., Leaper, R., Lefebvre, W., Lenton, A., Lynch, A., Metzl, N., Murray, A., O'Farrell, S., Peck, L., Pörtner, H., Roscoe, H., Smale, D., Smetacek, V., Summerhayes, C., Turner, J., Vanreusel, A., Vaughan, D., Verde, C., Wang, Z., 2009. The next 100 years. In: Turner, J., Convey, P., Prisco, G.D., Mayewski, P.A., Hodgson, D.A., Fahrbach, E., Bindschadler, R., Gutt, J. (Eds.), Antarctic Climate Change and the Environment - A Contribution to the International Polar Year 2007–2008. Scientific Committee on Antarctic Research, Cambridge, UK, pp. 299–388.

Bentley, M.J., The Raised Consortium, 2014. A community-based geological reconstruction of Antarctic ice sheet deglaciation since the last glacial maximum. Quat. Sci. Rev. 100, 1–9.

Berger, A., 1988. Milankovitch theory and climate. Rev. Geophys. 26 (4), 624–657.

Berger, A., Loutre, M.F., 1991. Insolation values for the climate of the last 10 million years. Quat. Sci. Rev. 10 (4), 297–317.

Bintanja, R., van Oldenborgh, G.J., Drijfhout, S.S., Wouters, B., Katsman, C.A., 2013. Important role for ocean warming and increased ice-shelf melt in Antarctic sea-ice expansion. Nat. Geosci. 6, 376–379.

Campagne, P., Crosta, X., Schmidt, S., Houssais, M.H., Ther, O., Massé, G., 2016. Sedimentary response to sea-ice and atmospheric variability over the instrumental period off Adélie Land, East Antarctica. Biogeosciences 13, 4205–4218.

Cape, M.R., Vernet, M., Skvarca, P., Marinsek, S., Scambos, T., Domack, E., 2015. Foehn winds link climate-driven warming to ice shelf evolution in Antarctica. J. Geophys. Res. Atmos. 120, 11,037–11,057.

Chapman, W.L., Walsh, J.E., 2007. A synthesis of Antarctic temperatures. J. Clim. 20, 4096–4117.

Cobb, K.M., Westphal, N., Sayani, H.R., Watson, J.T., Di Lorenzo, E., Cheng, H., Edwards, R.L., Charles, C.D., 2013. Highly variable El Niño-Southern Oscillation throughout the Holocene. Science 339, 67–70.

Compo, G.P., Whitaker, J.S., Sadershmukh, P.D., Matsui, N., Allan, R.J., Yin, X., Gleason, B.E., Vose, R.S., Rutledge, G., Bessemoulin, P., Brönniman, S., Brunet, M., Crouthamel, R.I., Grant, A.N., Groisman, P.Y., Jones, P.D., Krul, M.C., Kruger, A.C., Marshall, G.J., Maugeri, M., Mok, H.Y., Nordli, O., Ross, T.F., Trigo, R.M., Wang, X.L., Woodruff, S.D., Worley, S.J., 2011. The Twentieth Century Reanalysis Project. Q. J. R. Meteorol. Soc. 137 (654), 1–28.

Conroy, J.L., Overpeck, J.T., Cole, J.E., Shanahan, T.M., Steinitz-Kannan, M., 2008. Holocene changes in eastern tropical Pacific climate inferred from a Galapagos lake sediment record. Quat. Sci. Rev. 27, 1166–1180.

Cook, A.J., Fox, A.J., Vaughan, D.G., Ferrigno, J.G., 2005. Retreating glacier fronts on the Antarctic Peninsula over the past half-century. Science 308, 541–544.
Crespin, J., Yam, R., Crosta, X., Massé, G., Schmidt, S., Campagne, P., Shemesh, A., 2014. Holocene glacial discharge and recent instability in East Antarctica. Earth Planet. Sci. Lett. 394, 38–47.
Crosta, X., Debret, M., Denis, D., Courty, M.A., Ther, O., 2007. Holocene long- and short-term climate changes off Adélie Land, East Antarctica. G-Cubed 8 (11), Q11009. http://dx.doi.org/10.1029/2007GC001718.
Crosta, X., Denis, D., Ther, O., 2008. Sea ice seasonality during the Holocene, Adélie Land, East Antarctica. Mar. Micropaleontol. 66 (3–4), 222–232.
Cunningham, W., Leventer, A., Andrews, J.T., Jennings, A.E., Licht, K.J., 1999. Late Pleistocene-Holocene marine conditions in the Ross Sea, Antarctica: evidence from the diatom record. The Holocene 9 (2), 129–139.
Dash, M.K., Pandey, P.C., Vyas, N.K., Turner, J., 2013. Variability in the ENSO-induced southern hemispheric circulation and Antarctic sea ice extent. Int. J. Climatol. 33 (3), 778–783.
DeConto, R.M., Pollard, D., 2016. Contribution of Antarctica to past and future sea-level rise. Nature 531, 591–597.
Delworth, T.L., Zeng, F., 2008. Simulated Impact of Altered Southern Hemisphere Winds on the Atlantic Meridional Overturning Circulation. Geophys. Res. Lett. 35, L20708. http://dx.doi.org/10.21029/22008GL035166.
Denis, D., Crosta, X., Barbara, L., Massé, G., Renssen, H., Ther, O., Giraudeau, J., 2010. Sea ice and wind variability during the Holocene in East Antarctica: insight on middle-high latitude coupling. Quat. Sci. Rev. 29, 3709–3719.
Dufresne, J.-L., Foujols, M.-A., Denvil, S., Caubel, A., Marti, O., Aumont, O., Balkanski, Y., Bekki, S., Bellenge, H., Benshila, R., Bony, S., Bopp, L., Braconnot, P., Brockmann, P., Cadule, P., Cheruy, F., Codron, F., Cozic, A., Cugnet, D., de Noblet, N., Duvel, J.-P., Ethé, C., Fairhead, L., Fichefet, T., Flavoni, S., Friedlingstein, P., Grandpeix, J.-Y., Guez, L., Guilyardi, E., Hauglustaine, D., Hourdin, F., Idelkadi, A., Ghattas, J., Joussaume, S., Kageyama, M., Krinner, G., Labetoulle, S., Lahellec, A., Lefebvre, M.-P., Lefevre, F., Levy, C., Li, Z.X., Lloyd, J., Lott, F., Madec, G., Mancip, M., Marchand, M., Masson, S., Meurdesoif, Y., Mignot, J., Musat, I., Parouty, S., Polcher, J., Rio, C., Schulz, M., Swingedouw, D., Szopa, S., Talandier, C., Terray, P., Viovy, N., Vuichard, N., 2013. Climate change projections using the IPSL-CM5 earth system model: from CMIP3 to CMIP5. Clim. Dyn. 40 (9–10), 2123–2165.
Emile-Geay, J., Cobb, K.M., Carré, M., Braconnot, P., Leloup, J., Zhou, Y., Harrison, S.P., Corrège, T., McGregor, H.V., Collins, M., Driscoll, R., Elliot, M., Schneider, B., Tudhope, A., 2015. Links between tropical Pacific seasonal, interannual and orbital variability during the Holocene. Nat. Geosci. 9, 168–173.
Etourneau, J., Collins, L.G., Willmott, V., Kim, J.H., Barbara, L., Leventer, A., Domack, E., Schouten, S., Sinninghé Damsté, J.S., Klein, V., Crosta, X., Massé, G., 2013. Holocene climate variations in the western Antarctic Peninsula: evidence for sea ice extent predominantly controlled by changes in insolation and ENSO variability. Clim. Past 9, 1431–1446.
Foldvik, A., Gammelsrød, T., Østerhus, S., Fahrbach, E., Rohardt, G., Schröder, M., Nicholls, K.W., Padman, L., Woodgate, R.A., 2004. Ice shelf water overflow and bottom water formation in the southern Weddell Sea. J. Geophys. Res. 109, C02015. http://dx.doi.org/10.1029/2003JC002008.
Franzke, C., 2013. Significant reduction of cold temperature extremes at Faraday/ Vernadsky station in the Antarctic Peninsula. Int. J. Climatol. 33, 1070–1078.
Gersonde, R., Zielinski, U., 2000. The reconstruction of late quaternary Antarctic Sea-ice distribution - the use of diatoms as a proxy for sea-ice. Palaeogeogr. Palaeoclimatol. Palaeoecol. 162, 263–286.
Golledge, N.R., Kowalewski, D.E., Naish, T.R., Levy, R.H., Fogwill, C.J., Gasson, E.G.W., 2015. The multi-millennial Antarctic commitment to future sea-level rise. Nature 526, 421–425.
Harris, P., Taylor, F., Pushina, Z., Leitchenkov, G., O'Brien, P.E., Smirnov, V., 1998. Lithofacies distribution in relation to the geomorphic provinces of Prydz Bay. East Antarct. Antarct. Sci. 10 (3), 227–235.
Hemer, M.A., Harris, P.T., 2003. Sediment core from beneath the Amery Ice Shelf, East Antarctica, suggest mid-Holocene ice-shelf retreat. Geology 31 (2), 127–130.
Hemer, M.A., Post, A.L., O'Brien, P.E., Craven, M., Truswell, E.M., Roberts, D., Harris, P.T., 2007. Sedimentological signatures of the sub-Amery Ice Shelf circulation. Antarct. Sci. 19 (4), 497–506.
Heroy, D.C., Anderson, J.B., 2007. Radiocarbon constraints on Antarctic peninsula ice sheet retreat following the last glacial maximum (LGM). Quat. Sci. Rev. 26, 3286–3297.
Herraiz-Borreguero, L., Coleman, R., Allison, I., Rintoul, S.R., Craven, M., Williams, G.D., 2015. Circulation of modified Circumpolar Deep Water and basal melt beneath the Amery Ice Shelf, East Antarctica. J. Geophys. Res. Oceans 120, 3098–3112.
Hodgson, D.A., Abram, N., Anderson, J., Bargelloni, P., Barrett, P., Bentley, M.J., Bertler, N.A.N., Chown, S., Clarke, A., Convey, P., Crame, A., Crosta, X., Curran, M., Prisco, G.D., Goodwin, I., Gutt, J., Massé, G., Masson-Delmotte, V., Mayewski, P.A., Mulvaney, R., Peck, L., Pörtner, H.O., Röthlisberger, R., Stevens, M.I., Summerhayes, C.P., van Ommen, T., Verde, C., Verleyen, E., Vyverman, W., Wiencke, C., 2009. Antarctic climate and environment history in the pre-instrumental period. In: Turner, J., Convey, P., Prisco, G.D., Mayewski, P.A., Hodgson, D.A., Fahrbach, E., Bindschadler, R., Gutt, J. (Eds.), Antarctic Climate Change and the Environment - A Contribution to the International Polar Year 2007–2008. Scientific Committee for Antarctic Research, Cambridge, UK, pp. 115–181.
Holland, P.R., Jenkins, A., Holland, D.M., 2008. The response of ice shelf basal melting to variations in ocean temperature. J. Clim. 21, 2558–2572.
Ingólfsson, O., Hjort, C., Berkman, P.A., Björck, S., Colhoun, E., Goodwin, I.D., Hall, B., Hirakawa, K., Melles, M., Möller, P., Prentice, M.L., 1998. Antarctic glacial history since the last glacial maximum: an overview of the record on land. Antarct. Sci. 10 (3), 326–344.
Jones, J.M., Gille, S.T., Goosse, H., Abram, N.J., Canziani, P.O., Charman, D.J., Clem, K.R., Crosta, X., Lavergne, C.d., Eisenman, I., England, M.H., Fogt, R.L., Frankcombe, L.M., Marshall, G.J., Masson-Delmotte, V., Morrison, A.K., Orsi, A.J., Raphael, M.N., Renwick, J.A., Schneider, D.P., Simpkins, G.R., Steig, E.J., Stenni, B., Swingedouw, D., Vance, T.R., 2016. Assessing recent trends in high-latitude southern hemisphere surface climate. Nat. Clim. Chang. 6, 917–926. http://dx.doi.org/10.1038/NCLIMATE3103.
Kim, J.H., van der Meer, J., Schouten, S., Helmke, P., Willmott, V., Sangiorgi, F., Koç, N., Hopmans, E.C., Damsté, J.S.S., 2010. New indices and calibrations derived from the distribution of crenarchaeal isoprenoid tetraether lipids: implications for past sea surface temperature reconstructions. Geochim. Cosmochim. Acta 74, 4639–4654.
Kim, J.H., Crosta, X., Willmott, V., Renssen, H., Bonnin, J., Helmke, P., Schouten, S., Sinninghe Damsté, J.S., 2012. Holocene subsurface temperature variability in the eastern Antarctic continental margin. Geophys. Res. Lett. 39, L06705. http://dx.doi.org/10.1029/2012GL051157.
König-Langlo, G., King, J.C., Pettré, P., 1998. Climatology of the three coastal Antarctic stations Dumont d'Urville, Neumayer, and Halley. J. Geophys. Res. 103 (D9), 10,935–910,946.
Lamy, F., Kilian, R., Arz, H.W., François, J.P., Kaiser, J., Prange, M., Steinke, T., 2010. Holocene changes in the position and intensity of the southern westerly wind belt. Nat. Geosci. 3, 695–699.
Lazeroms, W.M.J., Jenkins, A., Gudmundsson, G.H., van de wal, R.S.W., 2018. Modelling present-day basal melt rates for Antarctic ice shelves using a parametrization of buoyant meltwater plumes. Cryosphere 12, 49–70.
Lenaerts, J.T.M., Lhermitte, S., Drews, R., Ligtenberg, S.R.M., Berger, S., Helm, V., Smeets, C.J.P.P., van den Broeke, M.R., van den Berg, W.J., van Meijgaard, E., Eijkelboom, M., Eisen, O., Pattyn, F., 2016. Meltwater produced by wind-albedo interaction stored in an East Antarctica ice shelf. Nat. Clim. Chang. 7, 58–63.
Leventer, A., Domack, E.W., Dunbar, R., Pike, J., Stickley, C., Maddison, E., Brachfeld, S., Manley, P., McClennen, C.E., 2006. Marine sediment record from the East Antarctic margin reveals dynamics of ice sheet recession. GSA Today 16 (12), 4–10.
Liu, C., Wang, Z., Cheng, C., Xia, R., Li, B., Xie, Z., 2017. Modeling modified Circumpolar Deep Water intrusions onto the Prydz Bay continental shelf, East Antarctica. J. Geophys. Res. Oceans 122, 5198–5217.
Mackinstosh, A.N., Golledge, N., Domack, E., Dunbar, R., Leventer, A., White, D., Pollard, D., DeConto, R., Fink, D., Zwartz, D., Gore, D.B., Lavoie, C., 2011. Retreat the East Antarctic Ice Sheet during the last glacial termination. Nat. Geosci. 4, 195–202.
Mackinstosh, A.N., Verleyen, E., O'Brien, P., White, D., McKay, R., Gore, D.B., Dunbar, R., Fink, D., Jones, R.S., Post, A.L., Miura, H., Leventer, A., Goodwin, I., Lilly, K., Crosta, X., Golledge, N., Wagner, B., Berg, S., van Ommen, T., Zwartz, D., Hodgson, D.A., Roberts, S.J., Vyverman, W., Massé, G., 2014. Retreat history of the East Antarctic Ice Sheet since the last glacial maximum. Quat. Sci. Rev. 100, 10–30.
Mahoney, A.R., Gough, A.J., Langhorne, P.J., Robinson, N.J., Stevens, C.L., Williams, M.J.M., Haskell, T.G., 2011. The seasonal appearance of ice shelf water in coastal Antarctica and its effect on sea ice growth. J. Geophys. Res. 116, C11032. http://dx.doi.org/10.1029/2011JC007060.
Makou, M.C., Eglinton, T.I., Oppo, D.W., Konrad, A.H., 2010. Postglacial changes in El Niño and La Niña behavior. Geology 38 (1), 43–46.
Masson, V., Vimeux, F., Jouzel, J., Morgan, V., Delmotte, M., Ciais, P., Hammer, C., Johnsen, S., Lipenkov, V.Y., Mosley-Thompson, E., Petit, J.R., Steig, E.J., Stievenard, M., Vaikmae, R., 2000. Holocene climate variability in Antarctica based on 11 ice-core isotopic records. Quat. Res. 54, 348–358.
Masson-Delmotte, V., Buiron, D., Ekaykin, A., Gallée, H., Jouzel, J., Krinner, G., Landais, A., Motoyama, H., Oerter, H., Pol, K., Ritz, C., Sime, L.C., Sodemann, H., Stenni, B., Uemera, R., Vimeux, F., 2011. A comparison of the present and last interglacial periods in six Antarctic ice cores. Clim. Past 7, 397–423.
Mayewski, P., Meredith, M.P., Summerhayes, C.P., Turner, J., Worby, A., Barrett, P.J., Casassa, G., Bertler, N.A.N., Bracegirdle, T., Garabato, A.C.N., Bromwich, D., Campbell, H., Hamilton, G.S., Lyons, W.B., Maasch, K.A., Aoki, S., Xiao, C., van Ommen, T., 2009. State of the Antarctic and Southern Ocean climate system. Rev. Geophys. 47, RG1003. http://dx.doi.org/10.1029/2007RG000231.
Meredith, M.P., King, J.C., 2005. Rapid climate change in the ocean west of the Antarctica Peninsula during the second half of the 20th century. Geophys. Res. Lett. 32, L19604. http://dx.doi.org/10.11029/12005GL024042.
Meredith, M.P., Wallace, M.I., Stammerjohn, S.E., Renfrew, I.A., Clarke, A., Venables, H.J., Shoosmith, D.R., Souster, T., Leng, M.J., 2010. Changes in the freshwater composition of the upper ocean west of the Antarctic Peninsula during the first decade of the 21st century. Prog. Oceanogr. 87, 127–143.
Meredith, M.P., Venables, H.J., Clarke, A., Ducklow, H.W., Erickson, M., Leng, M.J., Lenaerts, J.T.M., Van Den Broeke, M.R., 2013. The freshwater system west of the Antarctic Peninsula: spatial and temporal changes. Am. Meteorol. Soc. 26, 1669–1684.
Miles, B.W.J., Stokes, C.R., Vieli, A., Cox, N.J., 2013. Rapid, climate-driven changes in outlet glaciers on the Pacific coast of East Antarctica. Nature 500, 563–567.
Moy, C.M., Seltzer, G.O., Rodbell, D.T., Anderson, D.M., 2002. Variability of El Niño/ Southern Oscillation activity at millennial timescales during the Holocene epoch. Nature 420, 162–165.
Nicolas, J.P., Vogelmann, A.M., Scott, R.C., Wilson, A.B., Cadeddu, M.P., Bromwich, D.H., Verlinde, J., Lubin, D., Russell, L.M., Jenkinson, C., Powers, H.H., Ryczek, M., Stone, G., Wille, J.D., 2017. January 2016 extensive summer melt in West Antarctica favoured by strong El Niño. Nat. Commun. 8, 1579. http://dx.doi.org/10.1038/ncomms15799.
Nitsche, F.O., Porter, D., Williams, G., Cougnon, E.A., Fraser, A.D., Correia, R., Guerrero, R., 2017. Bathymetric control of warm ocean water access along the East Antarctic margin. Geophys. Res. Lett. 44, 8693–8944.
Nunes-Vaz, R.A., Lennon, G.W., 1996. Physical oceanography of the Prydz Bay region of

Antarctic waters. Deep-Sea Res. 43 (5), 603–641.
Obase, T., Abe-Ouchi, A., Kusahara, K., Hasumi, H., Ohgaito, R., 2017. Responses of basal melting of Antarctic ice shelves to the climate forcing of the last glacial maximum and CO_2 doubling. J. Clim. 30, 3473–3497.
O'Brien, P.E., Goodwin, I., Forsberg, C.F., Cooper, A.K., Whitehead, J., 2007. Late Neogene ice drainage changes in Prydz Bay, East Antarctica and the interaction of Antarctic ice sheet evolution and climate. Palaeogeogr. Palaeoclimatol. Palaeoecol. 245, 390–410.
O'Cofaigh, C., Davies, B.J., Livingstone, S.J., Smith, J.A., Johnson, J.S., Hocking, E.P., Hodgson, D.A., Anderson, J.B., Bentley, M.J., Canals, M., Domack, E., Dowdeswell, J.A., Evans, J., Glasser, N.F., Hillenbrand, C.D., Larter, R.D., Roberts, S.J., Simms, A.R., 2014. Reconstruction of ice-sheet changes in the Antarctic Peninsula since the last glacial maximum. Quat. Sci. Rev. 100, 87–100.
Orsi, A.H., Whitworth, T., Nowlin, W.D., 1995. On the meridional extent and fronts of the Antarctic Circumpolar Current. Deep-Sea Res. 42 (5), 641–673.
Paillard, D., Labeyrie, L., Yiou, P., 1996. Macintosh program performs time-series analysis. Eos 77 (39), 379.
Peck, V.L., Allen, C.S., Kender, S., McClymont, E.R., Hodgson, D.A., 2015. Oceanographic variability on the West Antarctic Peninsula during the Holocene and the influence of upper circumpolar deep water. Quat. Sci. Rev. 119, 54–65.
Pike, J., Crosta, X., Maddison, E., Stickley, C., Denis, D., Barbara, L., Renssen, H., 2009. Observations on the relationship between the Antarctic coastal diatoms *Thalassiosira antarctica* Comber and *Porosira glacialis* (Grunow) Jørgensen and sea ice concentrations during the Late Quaternary. Mar. Micropaleontol. 73, 14–25.
Pike, J., Swann, G.E.A., Leng, M.J., Snelling, A.M., 2013. Glacial discharge along the West Antarctic Peninsula during the Holocene. Nat. Geosci. 6, 199–202.
Pritchard, H.D., Arthern, R.J., Vaughan, D.G., Edwards, L.A., 2009. Extensive dynamic thinning on the margins of the Greenland and Antarctic ice sheets. Nature 461, 971–975.
Rayner, N.A., Parker, D.E., Horton, E.B., Folland, C.K., Alexander, L.V., Rowell, D.P., Kent, E.C., Kaplan, E.C.K., 2003. Global analysis of sea surface temperature, sea ice, and night marine air temperatures since the late nineteenth century. J. Geophys. Res. 108 (D14). http://dx.doi.org/10.1029/2002JD002670.
Regan, H.C., Holland, P.R., Meredith, M.P., Pike, J., 2018. Sources, variability and fate of freshwater in the Bellinghausen Sea, Antarctica. Deep-Sea Res. I 133, 59–71.
Renssen, H., Goosse, H., Fichefet, T., Masson-Delmotte, V., Koç, N., 2005. Holocene climate evolution in the high-latitude southern hemisphere simulated by a coupled atmosphere-sea-ice-ocean-vegetation model. The Holocene 15 (7), 951–964.
Rignot, E., Jacob, S., Mouginot, J., Scheuchl, B., 2013. Ice-shelf melting around Antarctica. Nature 341, 266–270.
Ritz, C., Edwards, T.L., Durand, G., Payne, A.J., Peyraud, V., Hindmarsh, R.C.A., 2015. Potential sea-level rise from Antarctic ice-sheet instability constrained by observations. Nature 528, 115–118.
Shemesh, A., Charles, C.D., Fairbanks, R.G., 1992. Oxygen isotopes in biogenic silica: global changes in ocean temperature and isotopic composition. Science 256, 1434–1436.
Shemesh, A., Burckle, L.H., Hays, J.D., 1995. Late Pleistocene oxygen isotope records of biogenic silica from the Atlantic sector of the Southern Ocean. Paleoceanography 10 (2), 179–196.
Shemesh, A., Hodell, D., Crosta, X., Kanfoush, S., Charles, C., Guilderson, T., 2002. Sequence of events during the last deglaciation in Southern Ocean sediments and Antarctic ice cores. Paleoceanography 17 (4), 1056. http://dx.doi.org/10.1029/2000PA000599.
Shevenell, A.E., Ingalls, A.E., Domack, E.W., Kelly, C., 2011. Holocene Southern Ocean surface temperature variability west of the Antarctic Peninsula. Nature 470, 250–254.
Smith, N.R., Tréguer, P., 1994. Physical and chemical oceanography in the vicinity of Prydz Bay, Antarctica. In: El-Sayed, S.Z. (Ed.), Southern Ocean Ecology: The Biomass Perspective. Cambridge University Press, Cambridge, UK, pp. 25–45.
Smith, N.R., Zhaoquian, D., Kerry, K.R., Wright, S., 1984. Water masses and circulation in the region of Prydz Bay, Antarctica. Deep-Sea Res. 31 (9), 1121–1147.
Smith, J.A., Andersen, T.J., Shortt, M., Gaffmey, A.M., Truffer, M., Santon, T.P., Bindschadler, R., Dutrieux, P., Jenkins, A., Hillenbrand, C.D., Ehrmann, W., Corr, H.F.J., Farley, N., Crowhurst, S., Vaughan, D.G., 2017. Sub-ice-shelf sediments record history of twentieth-century retreat of Pine Island Glacier. Nature 541, 77–80.
Stenni, B., Curran, M.A.J., Abram, N.J., Orsi, A., Goursaud, S., Masson-Delmotte, V., Neukom, R., Goosse, H., Divine, D., van Ommen, T., Steig, E.J., Dixon, D.A., Thomas, E.R., Bertler, N.A.N., Isaksson, E., Ekaykin, A., Frezzotti, M., Werner, M., 2017. Antarctic climate variability at regional and continental scales over the last 2,000 years. Clim. Past 13, 1609–1634.
Swann, G.E.A., Leng, M.J., 2009. A review of diatom $\delta^{18}O$ in palaeoceanography. Quat. Sci. Rev. 28, 384–398.
Swann, G.E.A., Leng, M.J., Sloane, H.J., Maslin, M.A., 2008. Isotope offsets in marine diatom $\delta^{18}O$ over the last 200 ka. J. Quat. Sci. 23 (4), 389–400.
Swann, G.E.A., Pike, J., Snelling, A.M., Leng, M.J., Williams, M.C., 2013. Seasonally resolved diatom $\delta^{18}O$ records from the West Antarctic Peninsula over the last deglaciation. Earth Planet. Sci. Lett. 364, 12–23.
Swingedouw, D., Fichefet, T., Huybrechts, P., Goosse, H., Driesschaert, E., Loutre, M.F., 2008. Antarctic ice-sheet melting provides negative feedbacks on future climate warming. Geophys. Res. Lett. 35, L17705. http://dx.doi.org/10.1029/2008GL034410.
Swingedouw, D., Fichefet, T., Goosse, H., Loutre, M.F., 2009. Impact of transient freshwater releases in the Southern Ocean on the AMOC and climate. Clim. Dyn. 33. http://dx.doi.org/10.1007/s00382-008-0496-1.
Tamsitt, V., Drake, H.F., Morrison, A.K., Talley, L.D., Dufour, C.O., Gray, A.R., Griffies, S.M., Mazloff, M.R., Sarmiento, J.L., Wang, J., Weijer, W., 2017. Spiraling pathways of global deep waters to the surface of the Southern Ocean. Nat. Commun. 8, 172. http://dx.doi.org/10.1038/s41467-017-00197-0.
Turner, J., 2004. The El Niño-Southern Oscillation and Antarctica. Int. J. Climatol. 24, 1–31.
Turner, J., Colwell, S.R., Marshall, G.J., Lachlan-Cope, T.A., Carleton, A.M., Jones, P.D., Lagun, V., Reid, P.A., Iagovnika, S., 2005. Antarctic climate change during the last 50 years. Int. J. Climatol. 25, 279–294.
Turner, J., Lu, H., White, I., King, J.C., Philipps, T., Hosking, J.S., Bracegirdle, T.J., Marshall, G.J., Mulvaney, R., Deb, P., 2016. Absence of 21^{st} century warming on Antarctic Peninsula consistent with natural variability. Nature 535, 411–415.
Varma, V., Prange, M., Merkel, U., Lohmann, G., Pfeiffer, M., Renssen, H., Wagner, A., Wagner, S., Schulz, M., 2012. Holocene evolution of the southern hemisphere westerly winds in transient simulations with global climate models. Clim. Past 8, 391–402.
Verleyen, E., Hodgson, D.A., Sabbe, K., Cremer, H., Emslie, S.D., Gibson, J., Hall, B., Imura, S., Kudoh, S., Marshall, G.J., McMinn, A., Melles, M., Newman, L., Roberts, D., Roberts, S.J., Singh, S.M., Sterken, M., Tavernier, I., Verkulich, S., van de Vyver, E., Nieuwenhuyze, W.V., Wagner, B., Vyverman, W., 2011. Post-glacial regional climate variability along the East Antarctic coastal margin - evidence from shallow marine and coastal terrestrial records. Earth Sci. Rev. 104, 199–212.
Voigt, I., Chiessi, C.M., Prange, M., Mulitza, S., Groeneveld, J., Varma, V., Henrich, R., 2015. Holocene shifts of the southern westerlies across the South Atlantic. Paleoceanography 30, 39–51.
Voigt, I., Chiessi, C.M., Piola, A.R., Henrich, R., 2016. Holocene changes in Antarctic Intermediate Water flow strength in the Southwest Atlantic. Palaeogeogr. Palaeoclimatol. Palaeoecol. 463, 60–67.
Walker, C.C., Gardner, A.S., 2017. Rapid drawdown of Antarctica's Wordie Ice Shelf glaciers in response to ENSO/Southern Annular Mode-driven warming in the Southern Ocean. Earth Planet. Sci. Lett. 476, 100–110.
Walker, D.P., Brandon, M.A., Jenkins, A., Allen, J.T., Dowdeswell, J.A., Evans, J., 2007. Oceanic heat transport onto the Amundsen Sea shelf through a submarine glacial trough. Geophys. Res. Lett. 34, L02602. http://dx.doi.org/10.109/2066GL028154.
Williams, G.D., Herraiz-Borreguero, L., Roquet, F., Tamura, T., Ohshima, K.I., Fukamachi, Y., Fraser, A.D., Gao, L., Chen, H., McMahon, C.R., Harcourt, R., Hindell, M., 2016. The suppression of Antarctic bottom water formation by melting ice shelves in Prydz Bay. Nat. Commun. 7, 12577. http://dx.doi.org/10.1038/ncomms12577.
Worby, A.P., Massom, R.A., Allison, I., Lytle, V.I., Heil, P., 1998. East Antarctic sea ice: a review of its structure, properties and drift. Antarct. Res. Ser. 74, 41–67.
Yuan, X., 2004. ENSO-related impacts on Antarctic sea ice: a synthesis of phenomenon and mechanisms. Antarct. Sci. 16 (4), 415–425.
Zhang, Z.S., Leduc, G., Sachs, J.P., 2014. El Niño evolution during the Holocene revealed by a biomarker rain gauge in the Galapagos Islands. Earth Planet. Sci. Lett. 404, 420–434.